DETERMINATION OF THE COEFFICIENT OF ROLLING FRICTION OF A HOLLOW CYLINDER ROLLING ON A CURVED TRACK USING A SMARTPHONE'S SENSOR

PIMPAKARN LAOTREEPHET

Graduate School Srinakharinwirot University

2020

การหาค่าสัมประสิทธิ์ความเสียดทานกลิ้งของทรงกระบอกกลวงที่กลิ้งบนรางโค้งโดยใช้เซนเซอร์
ของสมาร์ทโฟน

พิมพกานต์ เหล่าตรีเพชร

ปริญญานิพนธ์นี้เป็นส่วนหนึ่งของการศึกษาตามหลักสูตร
การศึกษามหาบัณฑิต สาขาวิชาฟิสิกส์
คณะวิทยาศาสตร์ มหาวิทยาลัยศรีนครินทรวิโรฒ
ปีการศึกษา 2563

DETERMINATION OF THE COEFFICIENT OF ROLLING FRICTION

OF A HOLLOW CYLINDER ROLLING ON A CURVED TRACK

USING A SMARTPHONE'S SENSOR

PIMPAKARN LAOTREEPHET

A Thesis Submitted in Partial Fulfillment of the Requirements

for the Degree of MASTER OF EDUCATION

(Physics)

Faculty of Science, Srinakharinwirot University

2020

THE THESIS TITLED

DETERMINATION OF THE COEFFICIENT OF ROLLING FRICTION
OF A HOLLOW CYLINDER ROLLING ON A CURVED TRACK
USING A SMARTPHONE'S SENSOR

BY

PIMPAKARN LAOTREEPHET

HAS BEEN APPROVED BY THE GRADUATE SCHOOL IN PARTIAL FULFILLMENT
OF THE REQUIREMENTS FOR THE MASTER OF EDUCATION
IN PHYSICS AT SRINAKHARINWIROT UNIVERSITY

(Assoc. Prof. Dr. Chatchai Ekpanyaskul, MD.)
Dean of Graduate School

ORAL DEFENSE COMMITTEE

.... Major-advisor
(Asst. Prof. Dr.Chokchai Puttharugsa)

.... Chair
(Asst. Prof. Dr.Chawarat Siriwong)

.... Committee
(Dr.Supitch Khemmani)

Title DETERMINATION OF THE COEFFICIENT OF ROLLING FRICTION
OF A HOLLOW CYLINDER ROLLING ON A CURVED TRACK USING A SMARTPHONE'S SENSOR
Author PIMPAKARN LAOTREEPHET
Degree MASTER OF EDUCATION
Academic Year 2020
Thesis Advisor Assistant Professor Dr. Chokchai Puttharugsa

This research demonstrated a simple experiment for determining the coefficient of rolling friction of a hollow cylinder rolling on a curved track using a smartphone sensor. The rolling motion of a hollow cylinder, both uncovered and covered, with various materials (synthetic leather and sponge sheets) was studied theoretically and experimentally. The smartphone (iPhone 4s) was attached to the end of the hollow cylinder for recording the angular position and angular velocity via the Rolling Cylinder application. The results revealed that the coefficient of rolling friction depends on the velocity of the hollow cylinder. This experiment may provide to be an alternative method to determine the coefficient of rolling friction and help students to better understand rolling motion.

Keyword : Rolling Friction Coefficient, Rolling Motion, Smartphone sensor

ACKNOWLEDGEMENTS

First of all, I have to thank my research advisor, Asst. Prof. Dr. Chokchai Puttharugsa for the continuous support of my study and research. His guidance and encouragement throughout the processes and discussion are very important for me. I also thank to another instructor: Dr. Supitch Kaemmanee for giving me some interesting points and comments in order to improve my work. Without their assistance, this research would not have been completed. Furthermore, this work was financially supported by the Institute for the Promotion of Teaching Science and Technology (IPST), so I am extremely grateful. Finally, special thanks goes to my family, they supported me everything in all the time of my research.

PIMPAKARN LAOTREEPHET

TABLE OF CONTENTS

	Page
ABSTRACT	D
ACKNOWLEDGEMENTS	E
TABLE OF CONTENTS	F
LIST OF FIGURES	H
CHAPTER 1 INTRODUCTION	1
Background	1
Objectives of the research	2
Significance of the research	3
Scope of the research	3
CHAPTER 2 LITERATURE REVIEW	4
2.1 Rigid body and moment of inertia	4
2.2 Rolling motion of rigid body	6
2.3 Rolling friction	7
2.4 A cylinder rolling down an inclined plane with and without rolling friction	9
2.5 Sensors in a smartphone	12
2.6 Literature reviews	14
CHAPTER 3 RESEARCH METHODOLOGY	16
3.1 Calculations for rolling without slipping on a curved aluminum track of a cylindrical pipe experiment	16
3.2 Experimental setup	20
3.2.1 Equipment	20

3.2.2 Method for building a simple experimental setup of a cylindrical pipe rolling on a curved aluminum track 21

3.2.3 Rolling Cylinder application 22

3.2.4 Experimental method 22

CHAPTER 4 RESULT 24

CHAPTER 5 SUMMARY DISCUSSION AND SUGGESTION 32

5.1 Summary 32

5.2 Discussion 32

5.3 Suggestion 33

REFERENCES 35

Appendix 37

VITA 48

LIST OF FIGURES

Page

Figure 1. Example of rotational inertia of some simple shapes (Serway & Jewett, 2004, 304). 5

Figure 2. (a) Translational motion, (b) Rotation motion, and (c) Rolling without slipping (Serway & Jewett, 2004, 318). 6

Figure 3. A cylindrical object rotates with angle ϕ, the center of mass moves with a distance $s = \phi R$ (Serway & Jewett, 2004, 317). 7

Figure 4. A soft object rolling on a hard plane with elementary normal forces along the contact area (Vozdecký et al., 2014). 9

Figure 5. A schematic diagram of a cylinder rolling down an inclined plane without slipping (Phommarach et al., 2012). 10

Figure 6. A cylinder with the radius of R rolling down an inclined plane (Cross, 2015b). 11

Figure 7. (a) The three axis of the smartphone (iPhone) and (b) Operating mode of acceleration sensors (Vogt & Kuhn, 2012). 13

Figure 8. The Tait–Bryan angles for the smartphone (Pörn & Braskén, 2016) and (b) the operation of the smartphone gyroscope (de Jesus, Pérez, de Oliveira, & Sasaki, 2018). 13

Figure 9. Screen of the Magnetometer application of the smartphone (left) and the experimental setup (right). 14

Figure 10. Schematic diagrams illustrating the cylindrical pipe with an attached smartphone for rolling down. 17

Figure 11. Schematic diagrams illustrating the cylindrical pipe with an attached smartphone for rolling up. 19

Figure 12. (a) Slotted flat steel bars and equal angle steels as a supporter, (b) curved aluminum track with supporter, and (c) digital images of the cylindrical pipe covered with synthetic leather and sponge sheets 21

Figure 13. (a) Rolling Cylinder application symbol, and (b) Display of Rolling Cylinder application. 22

Figure 14. The experimental setup consisting of the curved aluminum track and the cylindrical pipe with an attached iPhone 4s. 23

Figure 15. The proceeded data as a function of time; (a) the angular position ϕ_c and angular velocity ω_c, (b) the angular displacement ϕ and angular velocity ω_c, (c) the angular displacement θ and angular velocity ω. The inset shows a schematic of the cylindrical pipe with synthetic leather rolling on the curved aluminum track. 26

Figure 16. (a) The angular displacement θ and (b) the angular velocity ω with respect to time for the cylindrical pipe with and without synthetic leather or sponge. 28

Figure 17. (a) Amplitude and (b) maximum ω as a function of time for the cylindrical pipe with and without synthetic leather or sponge. 29

Figure 18. Parameter μ_r as a function of the cylindrical pipe's velocity v at the middle of the track for the cylindrical pipe with and without synthetic leather or sponge. 31

CHAPTER 1
INTRODUCTION

Background

The rolling motion of a rigid body is one of topics for introductory physics both in high school and undergraduate physics courses. Generally, most textbooks describe static friction, which plays an important role in pure rolling motion, without considering rolling friction. This is because rolling friction is quite small compared with the value of static friction. When an object rolls without slipping on a horizontal plane, it will eventually stop rolling because of the energy loss. Since there is no relative motion at a contact point between the surface and the object in the tangential direction, with the energy dissipation arises from the static friction force as a result of rolling friction (Cross, 2015a). For rolling with slipping, the velocity at the contact point is nonzero, implying that the kinetic friction force dominates instead (Ambrosis, Malgieri, Mascheretti, & Onorato, 2015). In practice, the rolling friction force is not commonly measured. However, the effects of rolling friction have been studied by Cross (Cross, 2015b, 2017). He presented a simple method for investigating the coefficient of rolling friction of a ball rolling down and up an inclined plane. The concept relates to the deformation of the ball and the surface, which are not perfectly smooth. The resultant reaction force N can be implied that it acts to the ball ahead of the center of mass, shifted by a distance D, and a torque exerted by N can resist its angular velocity (Cross, 2017). Also, this concept has led to a method for finding the coefficient of rolling friction in the case of a ball rolling on a concave lens (Cross, 2016), a low bounce ball rolling on a horizontal surface (Cross, 2015c), and a spinning disk on a horizontal plane (Cross, 2018). Additionally, Mungan (Mungan, 2012) adapted the concept to demonstrate how to determine the coefficient of rolling friction of a wheeled cart. Besides deformation concerning rolling friction, Minkin and Sikes (Minkin & Sikes, 2018) studied the rolling friction of a steel ball on a wood track by considering the mechanical energy change, which equals the work done by the rolling frictional force. They usually used a high-speed camera and a motion detector to record experimental data. However, these devices require specific software and have a high price, especially the high speed camera. Also, the devices are not familiar to student. Alternatively, a smartphone is an interesting device because students can use it fluently. Moreover, the smartphone's sensor can be used with appropriate applications to record the experimental data. Therefore, the smartphone seems to be a suitable experimental tool for measuring the coefficient of rolling friction.

Nowadays, smartphones are regularly employed in physics laboratory classes since they are portable and convenient to use. Educational applications for the IOS and Android systems have been developed to record experimental data, such as Sensorlog, Rolling cylinder, Phyphox, and Physics Toolbox Magnetometer. This method can help students to easily understand and visualize concepts of physics phenomena. For example, Egri and Szabó analyzed the oscillations of a rolling cart by using smartphones and tablets (Egri & Szabó, 2015). Kapucu presented how to estimate the maximum of coefficient of static friction by using a smartphone to measure the angle of inclination (Kapucu, 2018). Other authors (Puttharugsa, Khemmani, Utayarat, & Luangtip, 2016; Wattanayotin, Puttharugsa, & Khemmani, 2017; Yan, Xia, Lan, & Xiao, 2017) studied a cylinder rolling with/without slipping down an inclined plane and determined the coefficients of static friction and kinetic friction without considering the coefficient of rolling friction. A smartphone application was used to record angular position and angular velocity.

In this research, we demonstrated the use of a smartphone sensor to measure the angular position and angular velocity of a hollow cylinder (a cylindrical pipe) rolling on a curved aluminum track for determining the coefficient of rolling friction and describing the cylinder's motion. We expect that this experimental setup can be instruction for studying the basic physics concept of rolling motion in high school as well as college.

Objectives of the research

1. To study theoretically rolling without slipping motion on a curved aluminum track of a hollow cylinder (a cylindrical pipe).

2. To design and build a simple experimental setup of a cylindrical pipe with and without materials (synthetic leather or sponge) rolling without slipping on a curved aluminum track and record an experimental data by using smartphone.

Significance of the research

We build an experimental setup to observe rolling motion on a curved track of a cylindrical pipe with and without materials (synthetic leather or sponge). A smartphone was used to be a part of our experimental setup for collecting the experimental data, and then the coefficient of rolling friction was calculated. This method can guide the concept of rolling friction to students. Also, physics teachers can perform our experiment in physics laboratory classes since it is simple, low-cost, and suitable for students.

Scope of the research

We studied the rolling without slipping motion on a curved aluminum track of a cylindrical pipe with and without materials (synthetic leather or sponge) by considering the coefficient of rolling friction. A smartphone (iPhone 4s) was an important device in our experiment for measuring an angular position and angular velocity of a cylindrical pipe by using Rolling Cylinder application.

CHAPTER 2
LITERATURE REVIEW

This chapter presents about related research that are important for our experiment in order to study the rolling without slipping motion on a curved aluminum track of a cylindrical pipe. It includes

2.1 Rigid body and moment of inertia,

2.2 Rolling motion of rigid body,

2.3 Rolling friction,

2.4 A cylinder rolling down an inclined plane with and without rolling friction,

2.5 Sensors in a smartphone,

2.6 Literature reviews.

2.1 Rigid body and moment of inertia

Rigid body consists of many connected particles inside it that can hold its body although there are external forces act on it (Serway & Jewett, 2004, 302-305). Generally, the rigid body can move in the same direction as all particles and rotate in circular motion around a body's axis. For rotation of the rigid body, moment of inertia is a measurement of an object's rotational resistance based on its direction of rotation, mass and distance from the rotational axis. It can be expressed as,

$$I = \sum_{i=1}^{n} m_i r_i^2 . \qquad (1)$$

where I is the moment of inertia of the system.

m_i is the mass of i^{th} particle.

r_i is the distance from i^{th} particle to the rotational axis.

A general form to define the moment of inertia of the object's mass M and volume V, it can be imagined that the object is divided into small elements which has mass Δm_i per element. The moment of inertia of the object can be written as,

$$I = \sum_{i} r_i^2 \Delta m_i . \qquad (2)$$

And take the limit of this summation as $\Delta m_i \rightarrow 0$, therefore it can be calculated by an integral method,

$$I = \lim_{\Delta m_i \rightarrow 0} \sum_i r_i^2 \Delta m_i = \int r^2 dm. \tag{3}$$

Let $\rho = \dfrac{M}{V}$ where ρ and V are the density and volume of the object, respectively. The small element's mass is $dm = \rho dV$ so Eq.(3) gives,

$$I = \int \rho r^2 dV. \tag{4}$$

For the homogenous object, ρ is constant. ρ can be called as *volumetric mass density* since it shows mass per unit volume. Figure 1 shows the moments of inertia for objects about some axes.

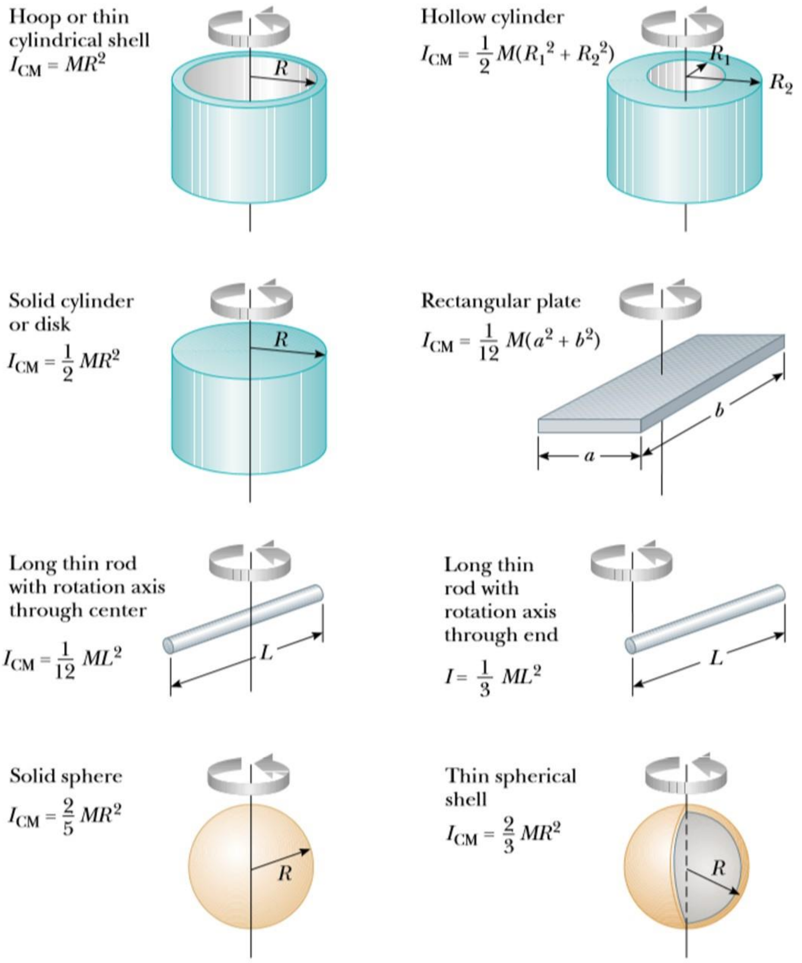

Figure 1. Example of rotational inertia of some simple shapes (Serway & Jewett, 2004, 304).

2.2 Rolling motion of rigid body

Rolling motion can be explain as the relation between translational and rotational motion in case, a contact point is at rest instantaneously. It is associated with forces and torques acting on a rolling object. As Figure 2, consider an object such as a ball, wheel, disc etc. moves on the horizontal plane and there is point P touching the surface. When the object moves as pure translational motion as shown in Figure 2(a), all points on the object move with the same velocity as the center of mass. It moves in a straight line without the external forces.

When the object moves as pure rotational motion about the center of mass, as shown in Figure 2(b). All points of the object move in circle about the axis of rotation. Its velocity is parallel to the tangent to the surface at point P and its magnitude is proportional to the distance from the rotational axis. Implying, a point at the center of rotation, it is at rest ($v_{\text{center of mass}} = 0$) and the outer edge has the maximum velocity called the tangential velocity.

In case, the object rolls without slipping on the horizontal plane as shown in Figure 2(c). The object moves and rotates in the same time. The contact point between object and surface is at rest relative to the surface therefore, velocity of this point becomes zero ($v_{\text{point of contact}} = 0$). There is no horizontal movement of the object at the contact point P, indicating static friction exists at P point.

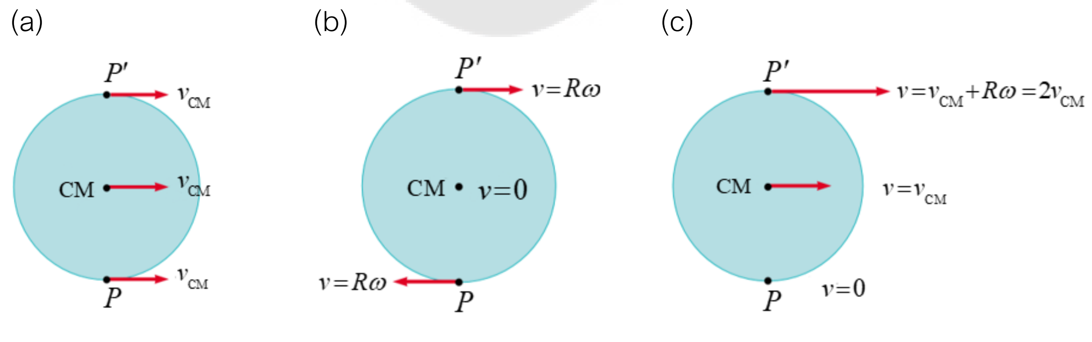

Figure 2. (a) Translational motion, (b) Rotation motion, and (c) Rolling without slipping (Serway & Jewett, 2004, 318).

Consider a uniform cylindrical object of radius R starts rolling without slipping on a flat surface as shown in Figure 3. As the cylindrical object rotates with angle ϕ, the center of mass moves with a distance s,

$$s = \phi R. \tag{5}$$

Therefore, translational speed (v_{cm}) of the center of mass for rolling object of radius R is given by

$$v_{\mathrm{CM}} = \frac{d\,s}{dt} = R\frac{d\phi}{dt} = R\omega. \tag{6}$$

where ω is the angular speed of the cylindrical object.

The magnitude of the linear acceleration (a_{CM}) of the center of mass for pure rolling motion is

$$a_{\mathrm{CM}} = \frac{d\,v_{\mathrm{CM}}}{dt} = R\frac{d\omega}{dt} = R\alpha. \tag{7}$$

where α is the angular acceleration of the cylindrical object.

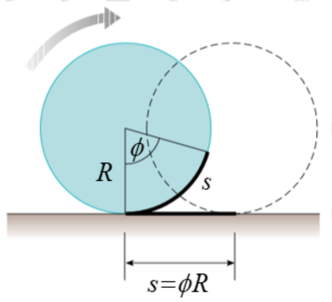

Figure 3. A cylindrical object rotates with angle ϕ, the center of mass moves with a distance $s = \phi R$ (Serway & Jewett, 2004, 317).

2.3 Rolling friction

Friction is defined as a force which opposes to an object's motion. Three modes of friction for solid surfaces are static friction, sliding friction, and rolling friction. Static friction force occurs when there is no relative motion between the object and the surface. Static friction force can remain the object stationary, so it is opposite to external forces acting on the object. For small external forces, the magnitude of the static force equals the magnitude of the external force. Until the external force exceeds the maximum force of static friction, the object will be in motion. The friction force for the object in motion is called sliding friction force or kinetic friction force. This friction force occurs when there is relative motion between the object and the surface. Sliding friction force opposes to the object's motion, and its value is typically less than the value of maximum static friction (Serway & Jewett, 2004, 131-133). Rolling friction force occurs when the object rolls over the surface. The contact area is quite small, as a result the value of rolling friction is much less than the value of static friction or sliding friction. Ideally, the energy loss for rolling friction is low, but in fact there are various causes for energy dissipation. It may be classified into 3 causes (Stolarski, 1990); the friction and micro-slip at the contact surface, the inelastic properties of the material and the roughness of the rolling surface.

In case of an object rolling without slipping on a horizontal plane, normally, the work done resulted from the static friction force is to reduce the translational energy. This work equals the work done resulted from the frictional torque which is to increase the rotational energy. Implying, there is energy transformation between the translational energy and rotational energy as a result of static friction force. Thus, there is no energy loss. Pure rolling cannot occur in the rolling of rough or deformable objects. When the object rolls along a linear distance with a constant speed, the resistance of rolling is called rolling friction. The deformation of materials is a dominant factor of rolling friction to dissipate energy. Elementary normal forces are perpendicular to the contact surface as shown in Fig.4. The resultant friction force must be opposite to translational velocity in order to decrease the translational velocity. Elementary forces acting to the object over the surface are asymmetric (Vozdecký, Bartoš, & Musilová, 2014). The resultant reaction force N acts to the object ahead of its center of mass, shifted by a distance of D. Also, the torque is to decelerate the angular speed of the rolling object. Therefore, the energy loss primarily arises from the internal friction which relates to the object's deformation (Cross, 2015b).

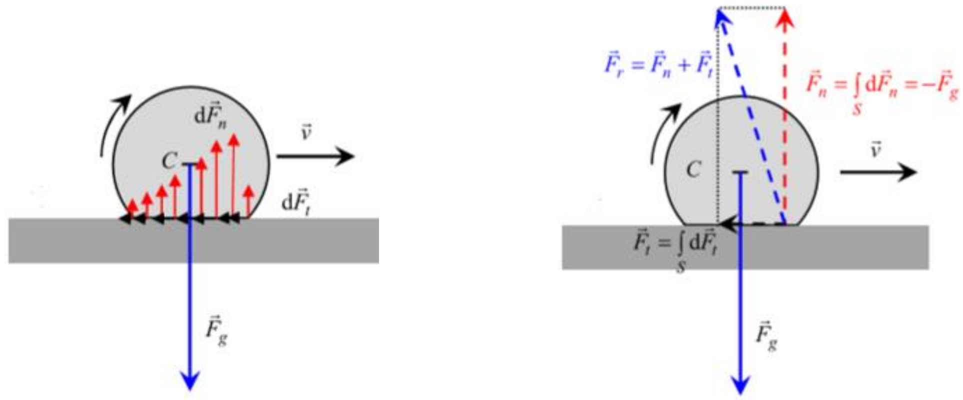

Figure 4. A soft object rolling on a hard plane with elementary normal forces along the contact area (Vozdecký et al., 2014).

2.4 A cylinder rolling down an inclined plane with and without rolling friction

Consider a cylinder with radius R and mass M rolling down (with $v=\omega R$) an inclined plane at angle θ with respect to the ground (see Figure 5). The angle θ and the cylinder's mass affect to the acceleration of the rolling cylinder according to the Newton's second law $\Sigma F = M\,a$ (Phommarach, Wattanakasiwich, & Johnston, 2012; Wattanayotin et al., 2017). The equations of motion can be represented as

$$Mg\sin\theta - f_s = M\frac{dv}{dt}, \tag{8}$$

and

$$N - Mg\cos\theta = 0. \tag{9}$$

Where f_s is the static force, and

N is the normal force acting on the object.

For the rotational component from $\Sigma\tau = I\alpha$ is also showed as

$$f_s R = I_{\mathrm{CM}}\frac{d\omega}{dt}. \tag{10}$$

Where $I_{\mathrm{CM}} = MR^2/2$ is the moment of inertia about the rotational axis of the cylinder.

By combination of Eq.(8)-(10) and the relation in Eq.(7), the acceleration can be determined as

$$a = \frac{2}{3}g\sin\theta, \tag{11}$$

And

$$f_s = \frac{1}{3} mg \sin\theta. \tag{12}$$

The friction force f_s have to be strong for preventing the cylinder from slipping. Therefore, a rolling without slipping condition can be written as

$$f_s \le \mu_s N. \tag{13}$$

Where $f_{s(\max)} = \mu_s N$ is the maximum static force, and

μ_s is the coefficient of static friction between the inclined plane and the cylinder.

Combining, Eq.(9), (12) and (13), we obtain

$$\mu_s \ge \frac{1}{3} \tan\theta. \tag{14}$$

Implying, the angle θ have to be less than some critical value, which is determined from Eq.(14). Thus, we obtain $\theta \le \tan^{-1}(3\mu_s)$ for a cylinder rolling without slipping down an inclined plane.

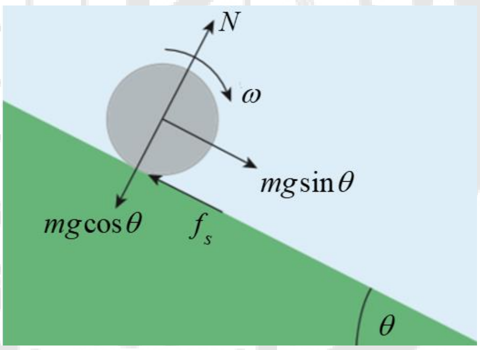

Figure 5. A schematic diagram of a cylinder rolling down an inclined plane without slipping (Phommarach et al., 2012).

In case of the soft cylinder rolling down an inclined plane without slipping, the rolling friction is more significant. As a consequence, the cylinder rolls slowly down with the reduced acceleration. The energy dissipation can arises from the internal friction f related to deformation of the surface and/or the rolling cylinder, as shown in Figure 6. There is compressed force at the cylinder's bottom. It is pressed down with a small distance x. Also, the normal force N acts over the contact surface but it is not uniformly distributed so the normal force can be implied that it acts to the cylinder ahead of its center of mass, shifted by a distance D (Cross, 2015b).

The equations of motion can be represented as

$$Mg\sin\theta - f = M\frac{dv}{dt}, \tag{15}$$

and

$$fR - ND = I_{\mathrm{CM}}\frac{d\omega}{dt}. \tag{16}$$

Where $I_{\mathrm{CM}} = MR^2/2$ is the moment of inertia about the rotational axis of a cylinder, and $N = Mg\cos\theta$ is the normal force acting on the cylinder.

By combination Eq.(15) and (16), it can be rewritten as,

$$\frac{dv}{dt} = \frac{2g}{3}\left(\sin\theta - \frac{D}{R}\cos\theta\right), \tag{17}$$

and

$$\mu_s = \frac{f}{N} = \frac{(\tan\theta/2 + D/R)}{3/2}. \tag{18}$$

where μ_s is the coefficient of static friction and it can be defined as a ratio f/N. μ_s is varied by θ. Indeed, the first term of μ_s vanishes when the cylinder rolls on the horizontal plane because θ is zero. While, the second term $\mu_r = 2D/3R$ is represented as the coefficient of rolling friction. The cylinder rolling on the inclined plane, D/R can be ignored because it is very small compared to the first term of μ_s.

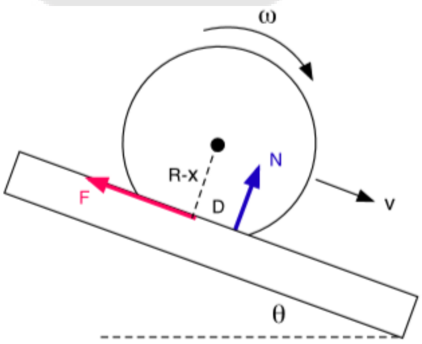

Figure 6. A cylinder with the radius of R rolling down an inclined plane (Cross, 2015b).

Consider the object rolling without slipping on a flat surface, the rolling friction can be obtained from Eq.(18),

$$f = \mu_r Mg = -Mdv/dt = \frac{2MgD}{3R}. \tag{19}$$

The translational energy decreases in 1 cycle given by

$$\Delta(0.5Mv^2) = f \times 2\pi R = 2\pi \frac{2MgD}{3}. \tag{20}$$

The decrease in the rotational energy (1 cycle) equals 2π multiplied by the net torque of the object. For the horizontal surface, $\theta = 0$ so Eq.(20) can be rewritten as

$$\Delta(0.5I_{\text{CM}}\omega^2) = I_{\text{CM}} \frac{d\omega}{dt} \times 2\pi = 2\pi \frac{MgD}{3}. \tag{21}$$

Therefore, the total energy loss equals $2\pi MgD$ for 1 revolution. This net loss resulted from torque ND is to decrease the rotational energy. The D value is proportional to μ_r so the energy loss is directly affected by μ_r, and also f. The work done by the frictional force and resultant normal force are considered to identify the mechanism of energy loss.

2.5 Sensors in a smartphone

A sensor in a smartphone is an electronic device for detecting and responding the change of physical environment. All data can be sent to the operating system. Nowadays, smartphones have been to develop, there are different type of sensors in the smartphone. The smartphone with the application is used to be an alternative tool in various physics experiment in order to receive the experimental data instead of using expensive devices. For example, accelerometer, gyroscope sensor, magnetometer.

2.5.1 Accelerometer

Accelerometer is used to measure acceleration and determine the movement along the three axis (x, y and z axis) of the smartphone (see Figure 7(a)). Various types of MEMS accelerometer hardware are available for the accelerometer for example, piezoelectric, which change the voltage if it is vibrated, or the differential capacitance, for the movement of silicon sheets. Figure 7(b) shows an example of a structure of two capacitors (connected with springs) for detecting the movement and convert into an acceleration value.

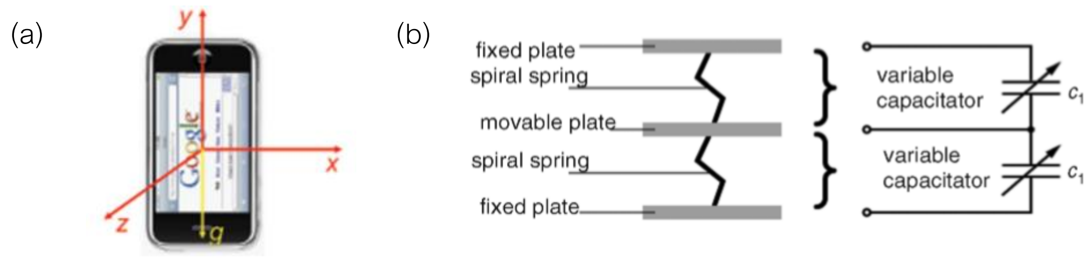

Figure 7. (a) The three axis of the smartphone (iPhone) and (b) Operating mode of acceleration sensors (Vogt & Kuhn, 2012).

2.5.2 Gyroscope sensor

Gyroscope sensor is developed from the accelerometer (rotation rate) to detect the change in orientation and also measure the angular velocity around three axis (x, y and z axis) of the smartphone (Figure 8(a)). The gravity of the Earth is used to determine the orientation. Figure 8(b) shows an example of the operating gyroscope experiment which is developed from MEMS (Micro electro mechanical systems) based on Coriolis effect (Pörn & Braskén, 2016). The rotation rate of the sensor is converted to an electric signal which is used to calculate the angular rate values.

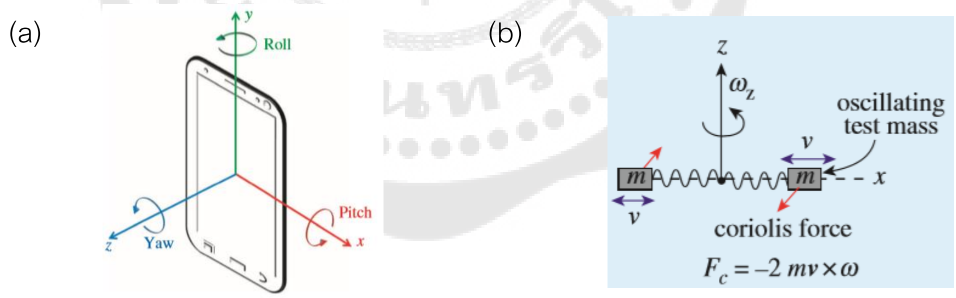

Figure 8. The Tait–Bryan angles for the smartphone (Pörn & Braskén, 2016) and (b) the operation of the smartphone gyroscope (de Jesus, Pérez, de Oliveira, & Sasaki, 2018).

2.5.3 Magnetometer

Magnetometer is used for measuring the strength of the magnetic fields. The Earth's magnetic field is a reference to determine the magnetic field intensity in the environment. Hall-effect sensor of the smartphone is used to detect the magnetic field along three perpendicular axis. The sensed voltage in the smartphone is converted to digital signal for giving the magnetic field intensity. Figure 8 shows an example of using magnetometer of the smartphone for detecting the magnetic field intensity via the application (Arabasi & Al-Taani, 2016).

Figure 9. Screen of the Magnetometer application of the smartphone (left) and the experimental setup (right).

2.6 Literature reviews

In 2015, Cross presented the simple experiment to describe the measurement of the coefficient of rolling friction. He expressed equations of motion of the object rolling on the flat surface and developed this concept to describe the object rolling down (Cross, 2015b) and up the inclined plane (Cross, 2017). Numerical method was used to compare with experimental results in order to find important parameters for calculating the energy loss from the coefficient of rolling friction. Additionally, the object rolling uphill and downhill on the concave lens (Cross, 2016) was studied by applying the previous methods and represented this system as two equations of motion in case of the object rolling down and up the concave lens. In this experiment, he used a camera to measure the oscillation amplitude of the cylinder in order to estimate the coefficient of rolling friction. Indicating that the coefficient of rolling friction is proportional to the ball's speed, and also inversely proportional to the object's diameter. For a large diameter of the object, it had the small coefficient of rolling friction value so it was ignored for some cases.

In 2017, Yan, Xia, Lan and Xiao studied about a PVC cylinder rolling without slipping down a wooden inclined plane (an angle θ of inclination) (Yan et al., 2017). They measured the angular velocity ω and acceleration α by using a smartphone which was mounted on the cylinder. The experimental data was extracted from the Sensor Kinetics Pro application on the smartphone. They obtained the coefficient of kinetic friction from fitting the angular acceleration α as a function of θ. Theoretically, the angular acceleration depends on $\cos\theta$. Furthermore, they compared the experimental results of the rolling with and without slipping by considering the critical angle θ_c condition. For this research, they used the low cost instruments and the smartphone with an educational application that can be used in physics laboratory, since it is quite easy to explain the concept of rolling on an inclined plane.

In 2018, Minkin and Sikes studied about the rolling friction of a steel ball on a concave wood track by considering the change of mechanical energy which is concerned with the work done resulted from the rolling frictional force (Minkin & Sikes, 2018). A camera allowed them to detect the rolling ball motion and represented the relation between the position-time and velocity-time of the rolling ball. Also, the total distance of the rolling ball was computed by using PASCO software which gave the positive area under the velocity curve. They estimated the coefficient of rolling friction by combination all steps above.

In 2018, Kapucu represented how to use a smartphone sensor for measuring the maximum coefficient of static friction. He designed a simple experimental setup for students in physics laboratories. The experiment consists of a smartphone, a table or chair with different surfaces, and objects. The smartphone was placed on the flat object (they was on the chair). Then, he slowly inclined the chair until the smartphone and the flat object began to slide. The angle of inclination was recorded by using Physics Toolbox Sensor Suite application. The average of maximum coefficient of static friction from the tangent of the critical angle was calculated, which was 0.351 ± 0.002 for the wooded object on seating surface of the chair.

CHAPTER 3
RESEARCH METHODOLOGY

This chapter explains about research process for analyzing the rolling without slipping motion on a curved aluminum track of a cylindrical pipe. It includes

3.1 Calculations for rolling without slipping on a curved aluminum track of a cylindrical pipe experiment,

3.2 Experimental setup.

3.1 Calculations for rolling without slipping on a curved aluminum track of a cylindrical pipe experiment

For our calculations, we followed Cross's procedure (Cross, 2016) with some additional improvement for determining the coefficient of rolling friction.

Consider a cylindrical pipe attached a smartphone (iPhone 4s) rolling down/up a curved aluminum track. The cylindrical pipe rolls without slipping with angular velocity ω_c and speed $v = \omega_c R_c = \pm ds/dt$, where R_c is the cylindrical pipe's radius and $s = (R_0 - R_c)\theta$ is an arc length with respect to an angle θ from the vertical for the cylindrical pipe rolling on the track, and R_0 is the curved aluminum track's radius. For this case, s is positive when the value of θ is positive. The resultant reaction force and frictional force are N and f, respectively. We assume that N acts to the cylindrical pipe ahead of its center of mass, shifted by a distance D_d or D_u for rolling down and up, respectively. This is accounted for the rolling friction effect (Cross, 2016).

Consider a cylindrical pipe rolling down a curved aluminum track (see Figure 10). The cylindrical pipe rolls down with v and ω_c, which are positive. In this case, we obtain $v = -ds/dt$ and $dv/dt = R_c d\omega_c/dt = -d^2s/dt^2$. While the cylindrical pipe is rolling down, both v and ω_c are increasing. This implies that the friction force f exerted on the cylindrical pipe must be in the right direction for applying a torque increasing ω_c.

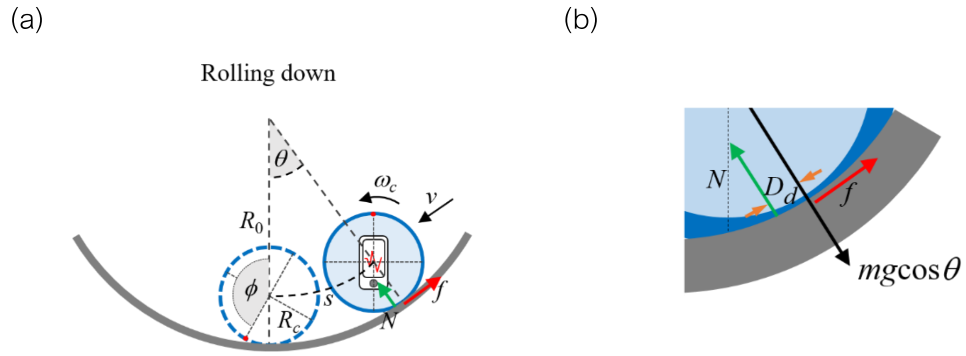

Figure 10. Schematic diagrams illustrating the cylindrical pipe with an attached smartphone for rolling down.

For the cylindrical pipe rolling down, the equations of motion can be expressed:

$$-Mg\sin\theta + f = M\frac{d^2s}{dt^2}, \tag{22}$$

and

$$f R_c - ND_d = I\frac{d\omega_c}{dt}. \tag{23}$$

where $M = m_c + m_f + m_i$ and $I = I_c + I_f + I_i = m_c R_c^2 + m_f R_f^2/2 + m_i\left(w^2 + l^2\right)/12$. The masses of the cylindrical pipe, circular foam board, and iPhone 4s are m_c, m_f, and m_i, respectively. The total moment of inertia (I) consists of the moments of inertia of the cylindrical pipe (I_c), circular foam board (I_f), and iPhone 4s (I_i), where w, l, and R_f are the width and length of the iPhone 4s, and the radius of the circular foam board, respectively.

Since the centripetal acceleration is much smaller than the g value, this is assumed that $N = Mg\cos\theta$ for a low speed of oscillation. For a low oscillation speed, we can assume that $\sin\theta \approx \theta$ and $\cos\theta \approx 1$. Then, we combine Eq.(22) and (23) to show that

$$\frac{d^2\theta}{dt^2} = -\frac{g(\theta - D_d/R_c)}{(R_0 - R_c)(1 + I/MR_c^2)}. \tag{24}$$

In order to simplify Eq.(24) let $y = \omega_0^2\left(\theta - D_d/R_c\right)$ and substitute this into Eq.(24), where

$$\omega_0^2 = \frac{g}{(R_0 - R_c)(1 + I/MR_c^2)}. \tag{25}$$

yielding

$$\frac{d^2y}{dt^2} = -\omega_0^2 y, \tag{26}$$

where ω_0 is the angular frequency of oscillation. Eq.(26) has a solution: $y = y_0 \cos(\omega_0 t)$. Then, we use the initial conditions at $t = 0, \theta = \theta_0$ and $d\theta/dt = 0$ to solve the equation, obtaining the angular displacement θ at any time:

$$\theta(t) = \frac{D_d}{R_c} + \left(\theta_0 - \frac{D_d}{R_c}\right)\cos(\omega_0 t). \tag{27}$$

We can express the angular velocity ω by the derivative of equation (27) with respect to t:

$$\omega(t) = -\omega_0\left(\theta_0 - \frac{D_d}{R_c}\right)\sin(\omega_0 t). \tag{28}$$

At the time that the cylindrical pipe arrives at the middle of the track (at $\theta = 0$), angular velocity is maximum, which is given an approximation by

$$\omega_{\max} = -\omega_0\left(\theta_0 - \frac{D_d}{R_c}\right) \to v_{\max} = -\omega_0\left(R_0 - R_c\right)\left(\theta_0 - \frac{D_d}{R_c}\right). \tag{29}$$

This is for $D_d/R_c << \theta_0$, the maximum velocity can be used as an initial condition for the cylindrical pipe rolling up the track.

For the cylindrical pipe rolling up the track (see Figure 11)), it can be seen that in this direction, v is positive and that f acts on the cylindrical pipe in the same direction as v. In this case, $v = ds/dt$ and $dv/dt = R_c d\omega_c/dt = d^2s/dt^2$. N acts to the cylindrical pipe ahead of its center of mass, shifted by a distance D_u. The equations of motion describing the cylindrical pipe rolling up the track are

$$Mg\sin\theta - f = -M\frac{d^2s}{dt^2}, \tag{30}$$

and

$$f R_c + ND_u = -I\frac{d\omega_c}{dt}. \tag{31}$$

Combining Eq.(30) and (31), we get

$$\frac{d^2\theta}{dt^2} = -\frac{g(\theta + D_d/R_c)}{(R_0 - R_c)(1 + I/MR_c^2)}. \tag{32}$$

Let $z = \omega_0^2\left(\theta + D_u/R_c\right)$, where

$$\omega_0^2 = \frac{g}{(R_0 - R_c)(1 + I/MR_c^2)}. \tag{33}$$

Substituting this into Eq.(32), we find that

$$\frac{d^2 z}{dt^2} = -\omega_0^2 z\ . \tag{34}$$

Again the solution of Eq.(34) is $z = z_0 \cos(\omega_0 t)$, and we assume that at $t = 0$, $\theta = 0$ and the maximum velocity is given an approximation by $v = \omega_0 (R_0 - R_c)(\theta_0 - D_d / R_c)$. The relevant solution of Eq.(32) is then

$$\theta(t) = \left(\theta_0 - \frac{D_d}{R_c}\right)\sin(\omega_0 t) + \frac{D_u}{R_c}\cos(\omega_0 t) - \frac{D_u}{R_c}. \tag{35}$$

We can express the angular velocity by the derivative of equation (35) with respect to t:

$$\omega(t) = \omega_0\left(\theta_0 - \frac{D_d}{R_c}\right)\cos(\omega_0 t) - \omega_0 \frac{D_u}{R_c}\sin(\omega_0 t). \tag{36}$$

(a) (b)

Figure 11. Schematic diagrams illustrating the cylindrical pipe with an attached smartphone for rolling up.

In summary, D/R_c values were estimated in each rolling cycle. From Eq.(28) for rolling down, ω is maximum when $\omega_0 t = \pi/2$ (the cylindrical pipe is rolling at the middle of the track). Therefore, $\omega = -\omega_0(\theta_0 - D_d / R_c)$ for every half cycle of rolling.

$$\frac{D_{d(n)}}{R_c} = \theta_{0(2n-1)} + \frac{\omega_{(2n-1)}}{\omega_0}\ . \tag{37}$$

where $n=1,2,3,...$ (n is the cycle of rolling). For rolling up, we consider Eq.(37) when $\omega_0 t = \pi / 2$ (the cylindrical pipe is at the rim of the track), so θ is maximum; therefore, θ will decrease by $\left(D_d / R_c\right)+\left(D_u / R_c\right)$ for every half cycle of rolling.

$$\frac{D_{u(n)}}{R_c} = \left(\theta_{0(2n-1)} - \theta_{0(2n)}\right) - \frac{D_{d(n)}}{R_c}. \tag{38}$$

where $n=1,2,3,...$ (n is the cycle of rolling). Note that, we consider the cylindrical pipe starts rolling down from right to left side of the track, it is accounted for the half cycle of rolling.

It is well known from previous work on an object rolling down an inclined plane (Cross, 2015b) that the friction force acting on the cylindrical pipe consists of two components. One component is the static frictional force, which depends on the inclined angle. The other component arises from D_d and D_u values (for rolling down and up, respectively) which are much smaller than the first component. They can be described as the rolling friction force or the rolling resistance. From the frictional force $\mu = f/N$ and combining the above equations, finally the coefficient of rolling friction was estimated by $\left(D_{d(n)}/R_c\right)/\left(1 + I/MR_c^2\right)$ and $\left(D_{u(n)}/R_c\right)/\left(1 + I/MR_c^2\right)$ for rolling down and up, respectively (Cross, 2017).

3.2 Experimental setup

3.2.1 Equipment

1. Aluminum sheet with a measuring tape, $0.350 \pm 0.001\ \mathrm{m}$ of width and $1.200 \pm 0.001\ \mathrm{m}$ of length.

2. Curved aluminum sheet supporter, consisting of slotted flat steel bars (10 pieces), equal angle steels (4 pieces) and screws.

Slotted flat steel bars are joined with screws; $1.000 \pm 0.001\ \mathrm{m}$ for horizontal length of track (2 pieces), $0.300 \pm 0.001\ \mathrm{m}$ for vertical length of track (4 pieces) and $0.350 \pm 0.001\ \mathrm{m}$ for width of track (4 pieces)

3. A smartphone (iPhone 4s) with its case, $0.122 \pm 0.001\ \mathrm{kg}$ of mass (m_i), $0.125 \pm 0.001\ \mathrm{m}$ of length (l) and $0.061 \pm 0.001\ \mathrm{m}$ of width (w).

4. A cylindrical pipe (PVC pipe), $0.522 \pm 0.001\ \mathrm{kg}$ of mass (m_c), $0.070 \pm 0.001\ \mathrm{m}$ of inner radius, $0.0753 \pm 0.0010\ \mathrm{m}$ of outer radius (R_c) and $0.134 \pm 0.001\ \mathrm{m}$ of height.

5. A circular foam board, $0.070 \pm 0.001\ \mathrm{m}$ of radius (R_f), $0.021 \pm 0.001\ \mathrm{m}$ of thickness and $0.004 \pm 0.001\ \mathrm{kg}$ of mass (m_f).

6. A synthetic leather (a thickness of $0.0070 \pm 0.0001\ \mathrm{m}$) and sponge sheets for covering PVC pipe.

7. Double sided sticky tape and scissors.

3.2.2 Method for building a simple experimental setup of a cylindrical pipe rolling on a curved aluminum track

Slotted flat steel bars and equal angle steels were connected together by screws as shown in Figure 12(a), and the curved aluminum track with the measuring tape was set on it (Figure 12(b)). In our experiment, we used double sided sticky tape for mounting iPhone 4s on the center of a circular foam board and put them on one side of the cylindrical pipe. Also, we covered the cylindrical pipe by a synthetic leather or sponge sheet as shown in Figure 12(c).

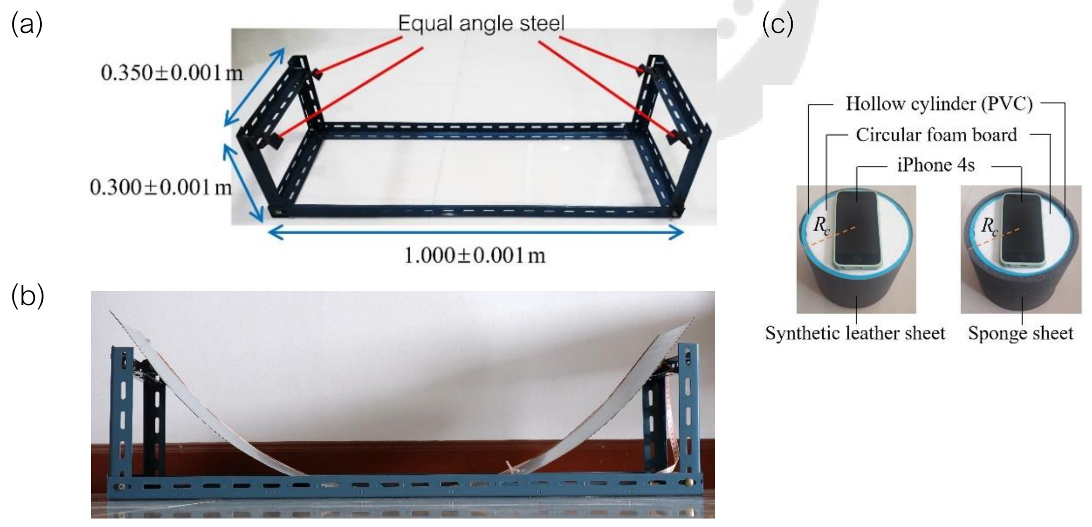

Figure 12. (a) Slotted flat steel bars and equal angle steels as a supporter, (b) curved aluminum track with supporter, and (c) digital images of the cylindrical pipe covered with synthetic leather and sponge sheets

3.2.3 Rolling Cylinder application

Rolling Cylinder application is free educational application developed by Ufuk Dilek. Features of this application are shown in Figure 13. It can be downloaded from App store for iPhone. Generally, smartphones have the motion sensor which can detect smartphone's movement in three dimensions and export data as position or velocity data to explain the motion of the smartphone. Rolling Cylinder application can be applied for experiment about rolling motion of a cylindrical object by fixing the smartphone to the object's base. When the object rotates, it will automatically record angular position and angular velocity at regular time intervals. All data is recorded as a CSV file, and users can export it via email. In CSV file, column A, B and C contain time (t), angular position (ϕ_c), and angular velocity (ω_c) of the cylindrical pipe, respectively.

(a)

(b)

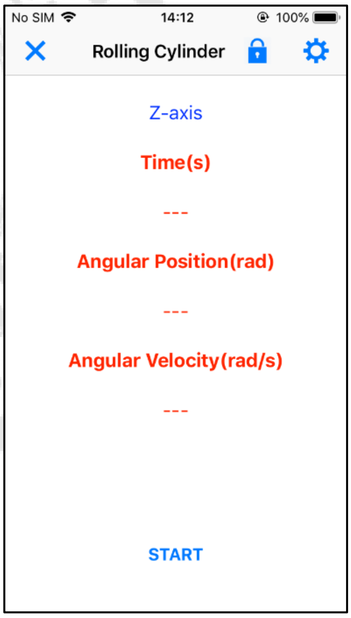

Figure 13. (a) Rolling Cylinder application symbol, and (b) Display of Rolling Cylinder application.

3.2.4 Experimental method

The curved track is made from an aluminum sheet; it is bent to be concave, as shown in Figure 14. The radius of the concave sheet (R_0) was measured by taking a photo of it and evaluating the ratio of the image scale to the actual scale from the photo, so $R_0 = 0.5133$ m. In the experiment, we released the cylindrical pipe with and without materials (synthetic leather and sponge) at a position of $s_0 = 0.15 \pm 0.02$ m . The smartphone was used to record simultaneously the angular position ϕ_c and angular velocity ω_c of the cylindrical pipe rolling down/up by using the Rolling Cylinder application. Then, we exported all data (a CSV file) via email. To analyze the experimental data, we expressed the angular displacement θ and angular velocity ω, corresponding to Eq.(27), (28), (35) and (36) by using $\theta = \phi R_c / (R_0 - R_c)$ and $\omega = \omega_c R_c / (R_0 - R_c)$. Note that $\theta = 0$ at the middle of the track, and $\phi = \phi_r - \phi_c$, where ϕ_r and ϕ_c are the angular position at the middle of the track and at any position on the track, respectively. In the analysis, we fitted a sinusoidal damped function to the experimental data in order to find the angular frequency (ω_0). Finally, the D values and the coefficient of rolling friction μ_r for the cylindrical pipe rolling down and up were estimated by $(D_d / R_c)/(1 + I/MR_c^2)$ and $(D_u / R_c)/(1 + I/MR_c^2)$, respectively.

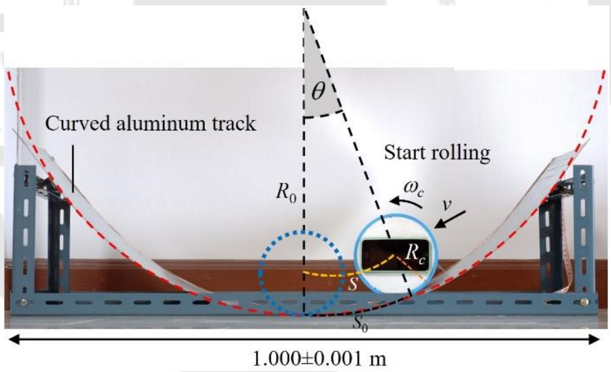

Figure 14. The experimental setup consisting of the curved aluminum track and the cylindrical pipe with an attached iPhone 4s.

CHAPTER 4
RESULT

The cylindrical pipe consists of the iPhone 4s mounted on the circular form board. $s_0 = 0.15 \pm 0.02\,\mathrm{m}$ in Figure 14 is a position for releasing the cylindrical pipe with various surface. $s_0 = \theta R_0$ is for rolling without slipping. At this position, the cylindrical pipe rolls without slipping along the curved track (see more details in appendix A). The angular position ϕ_c and angular velocity ω_c at regular time intervals are instantly measured and recorded by Rolling Cylinder application. This application records the angular position ϕ_c continuously, therefore the angular position can be recorded more than 2π rad, in case the cylindrical pipe rotation is greater than 1 cycle. The angular position will increase when the rotation of the cylindrical pipe is in a counterclockwise direction (it decreases for a clockwise direction). And the angular velocity ω_c are positive when the cylindrical pipe rotates in a counterclockwise direction (it is negative for a clockwise direction), so we can define the rotation's direction of the cylindrical pipe from the sign of experimental values.

Figure 15(a) shows raw data of the cylindrical pipe with synthetic leather (the synthetic leather cylinder), which was obtained from the Rolling Cylinder application. Time measurement for the synthetic leather cylinder from rest to stop was around $20\ \mathrm{s}$. It starts rolling with angular position $\phi_{c(A)} = 4.625\ \mathrm{rad}$ at point A. While the synthetic leather cylinder rolling down, ϕ_c increases until the synthetic leather cylinder reaches the middle of the track (the equilibrium position), where the angular position is equal to $6.475\ \mathrm{rad}$, denoted as ϕ_r (at point B). At this position, ϕ_r has the maximum angular velocity $\omega_{c(B)} = 5.832\ \mathrm{rad}$. Then, the synthetic leather cylinder is rolling up, and angular position also increases until point C of the curved track, where $\phi_{c(C)} = 8.129\ \mathrm{rad}$ and $\omega_c = 0$. After the synthetic leather cylinder reaches point C, it starts rolling down the curved track. The angular position ϕ_c decreases with increasing angular velocity ω_c in the opposite direction due to the synthetic leather cylinder rolling in clockwise direction.

Since the synthetic leather cylinder oscillates at point B (the equilibrium point), the angular displacement ϕ can be obtained by using $\phi = \phi_r - \phi_c$. Figure 15(b) illustrates the angular displacement ϕ with time of the synthetic leather cylinder. The synthetic leather cylinder oscillates at the middle of the track with the amplitude between $+1.849\,\mathrm{rad}$ (right side) and $-1.654\,\mathrm{rad}$ (left side). After that, the amplitude of the angular displacement decreases in each cycle because of the rolling friction until the synthetic leather cylinder stops rolling.

Figure 15(c) represents the angular displacement θ and angular velocity ω, which were changed from ϕ and ω_c, respectively, by using $\theta = \phi R_c / (R_0 - R_c)$ and $\omega = \omega_c R_c / (R_0 - R_c)$. Note that ω was multiplied by -1 to set positive values for the clockwise direction, since ω_c from the Rolling Cylinder application is recorded negative value in clockwise direction. Furthermore, it is obvious that ω leads to θ of $90°$. The fitting angular frequency ω_0 is $3.323\,\mathrm{rad/s}$, or the period is equal to $1.891\,\mathrm{s}$. The calculated ω_0 from Eq.(25) is equal to $3.469\,\mathrm{rad/s}$. Thus, about 4.2% is the error of these values. Figure 15(c) can provide the $D_{d(n)}/R_c$ and $D_{u(n)}/R_c$ values by using Eq.(37) and (38) for rolling down and up, respectively. These values will be further used for determining the coefficient of rolling friction by using $(D_{d(n)}/R_c)/(1 + I/MR_c^2)$ and $(D_{u(n)}/R_c)/(1 + I/MR_c^2)$ for rolling down and up, respectively.

Consider the first cycle or period ($n = 1$) for rolling down (at $t = 0$) at point A, the amplitude of the angular displacement is $\theta_{0(1)} = 0.318\,\mathrm{rad}$ with $\omega = 0$. When $\omega_0 t = \pi / 2$ at point B, the angular velocity increases to $\omega_{(1)} = -1.002\,\mathrm{rad/s}$ and $\theta = 0$. We used Eq.(37) to calculate the value of $D_{d(1)}/R_c$, which is 0.0163. For rolling up, the synthetic leather cylinder rolls from point B to C when $t = 0$ to $\omega_0 t = \pi/2$ (the 1st cycle of rolling up; $n = 1$). Then, it rolls up to $\theta_{0(2)} = -0.284\,\mathrm{rad}$ and $\omega = 0$. Obviously, the magnitude of θ for the synthetic leather cylinder rolling up is not equal to that for the synthetic leather cylinder rolling down. This is due to the rolling friction effect. According to Eq.(38), it indicates that $\theta_{0(n)}$ will decrease by a value of $(D_d/R_c) + (D_u/R_c)$ for each half cycle of rolling. Thus, the calculated value of $D_{u(1)}/R_c$ for rolling up is 0.0173. The calculation of D_1/R_c values for the synthetic leather cylinder rolling down or up is similar. Therefore, for the next cycles, the values of $D_{d(n)}/R_c$ and $D_{u(n)}/R_c$ can be calculated by alternately using Eq.(37) and (38) with a changing of n value.

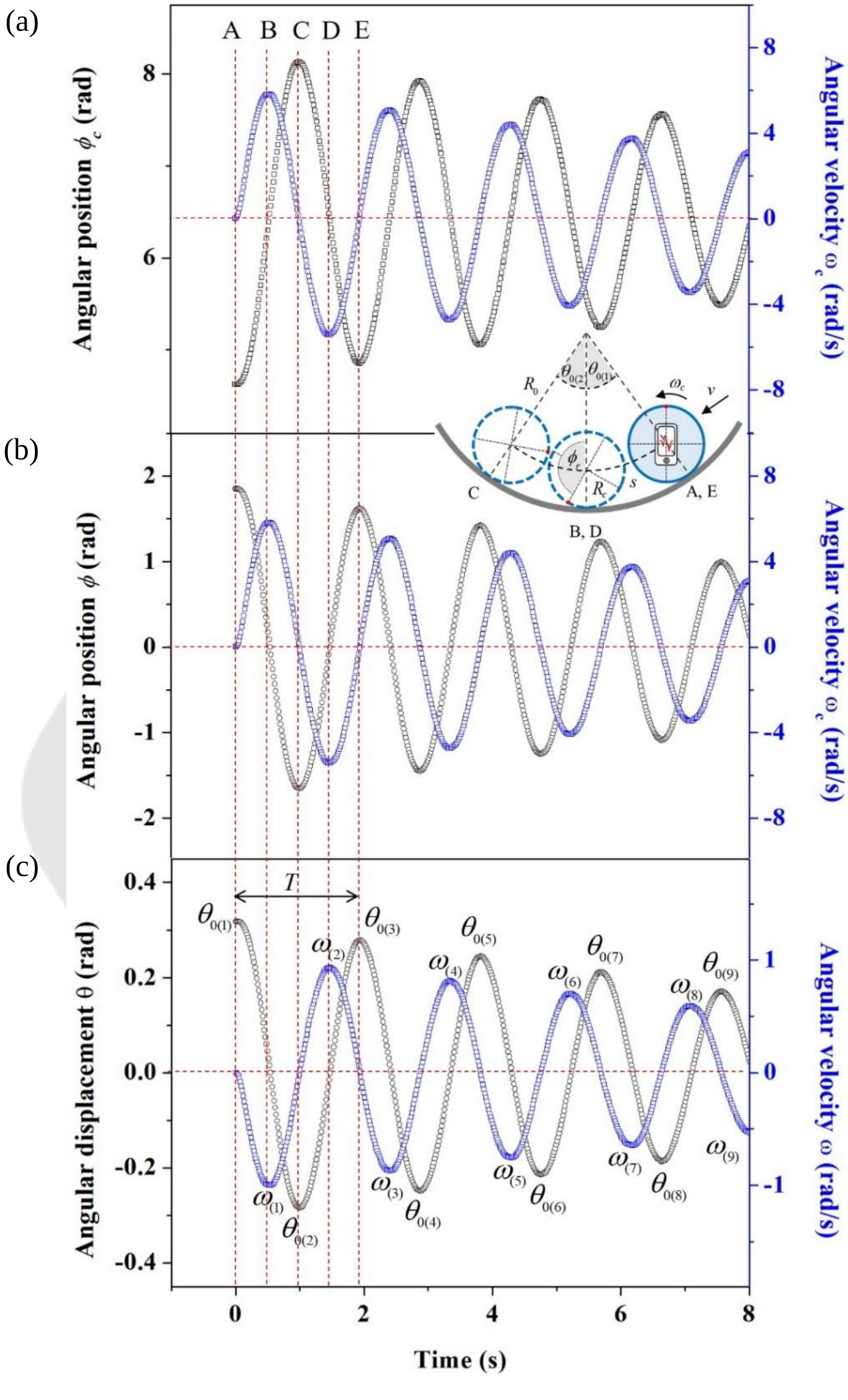

Figure 15. The proceeded data as a function of time; (a) the angular position ϕ_c and angular velocity ω_c, (b) the angular displacement ϕ and angular velocity ω_c, (c) the angular displacement θ and angular velocity ω. The inset shows a schematic of the cylindrical pipe with synthetic leather rolling on the curved aluminum track.

We repeated the experiment for three surfaces of the cylindrical pipe. The experimental results are shown in appendix B. Figure B1-B4, B5-B8 and B9-B17 are for the cylindrical pipe with synthetic leather, sponge, and the uncovered cylindrical pipe, respectively.

Figure 16 shows the angular displacement θ (Figure 16(a)) and angular velocity ω (Figure 16(b)) for three cylindrical pipe (with and without synthetic leather or sponge). All cylinders were released at the same position on the curved track. It can be seen that θ and ω of the cylindrical pipe with sponge (the sponge cylinder) significantly decrease when it is rolling in the 3rd cycle. Because the sponge surface is softer and thicker than the synthetic leather surface, it can be deformed easily. The sponge cylinder's angular displacement and angular velocity quickly decrease, and eventually it stops rolling within about $7\ \mathrm{s}$. In contrast, θ and ω of the synthetic leather cylinder gradually decrease with time due to its roughness. The effect of its thickness can be ignored since the synthetic leather surface is very thin. For the uncovered cylindrical pipe, θ and ω slightly decline because its roughness and thickness do not have a considerable effect on its rolling motion. However, all cylinders will eventually stop rolling due to the frictional force at the contact area.

Figure 17 shows the plot of the amplitude and the maximum ω with respect to time for the cylindrical pipe with various surfaces. It is clearly seen that both the amplitude and the maximum ω linearly decrease for the cylindrical pipe with synthetic leather or sponge, while they exponentially decrease for the uncovered cylindrical pipe. Moreover, time measurements for the cylindrical pipe with synthetic leather or sponge from rest to stop are around $20\mathrm{s}$ and $7\mathrm{s}$, respectively ($120\mathrm{s}$ is for the uncovered cylindrical pipe). Since the sponge surface is softer and thicker than the synthetic leather surface, the deformation plays a more significant role in stopping the cylinder.

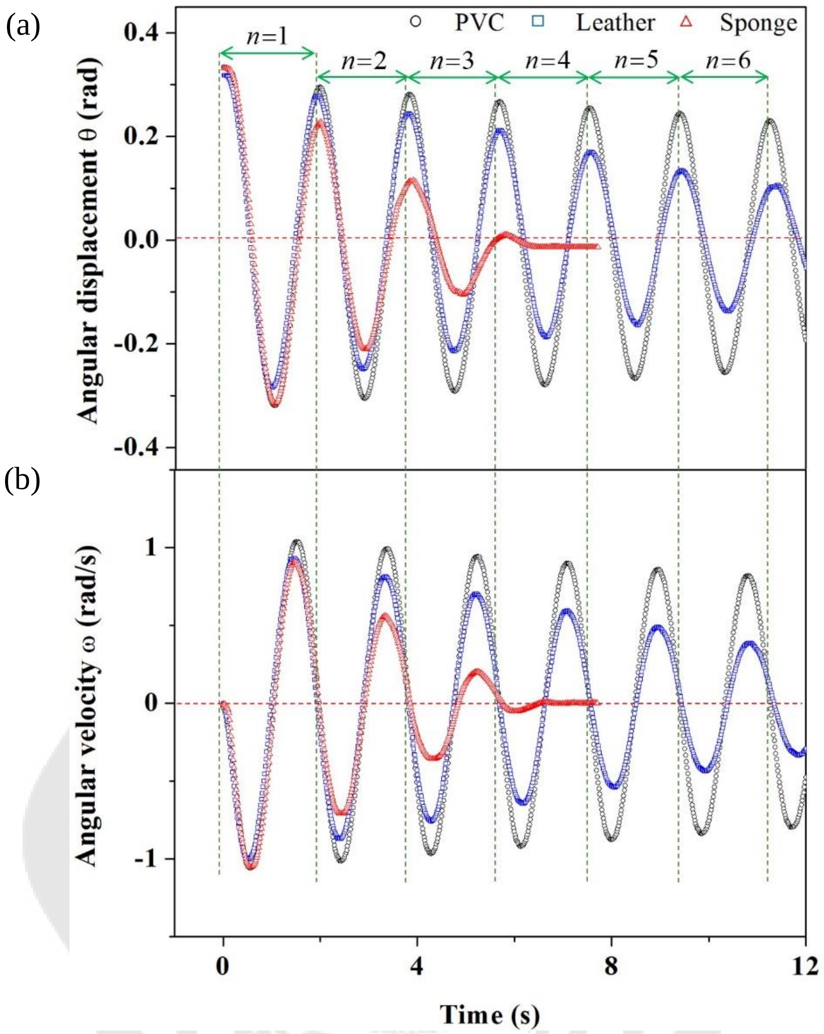

Figure 16. (a) The angular displacement θ and (b) the angular velocity ω with respect to time for the cylindrical pipe with and without synthetic leather or sponge.

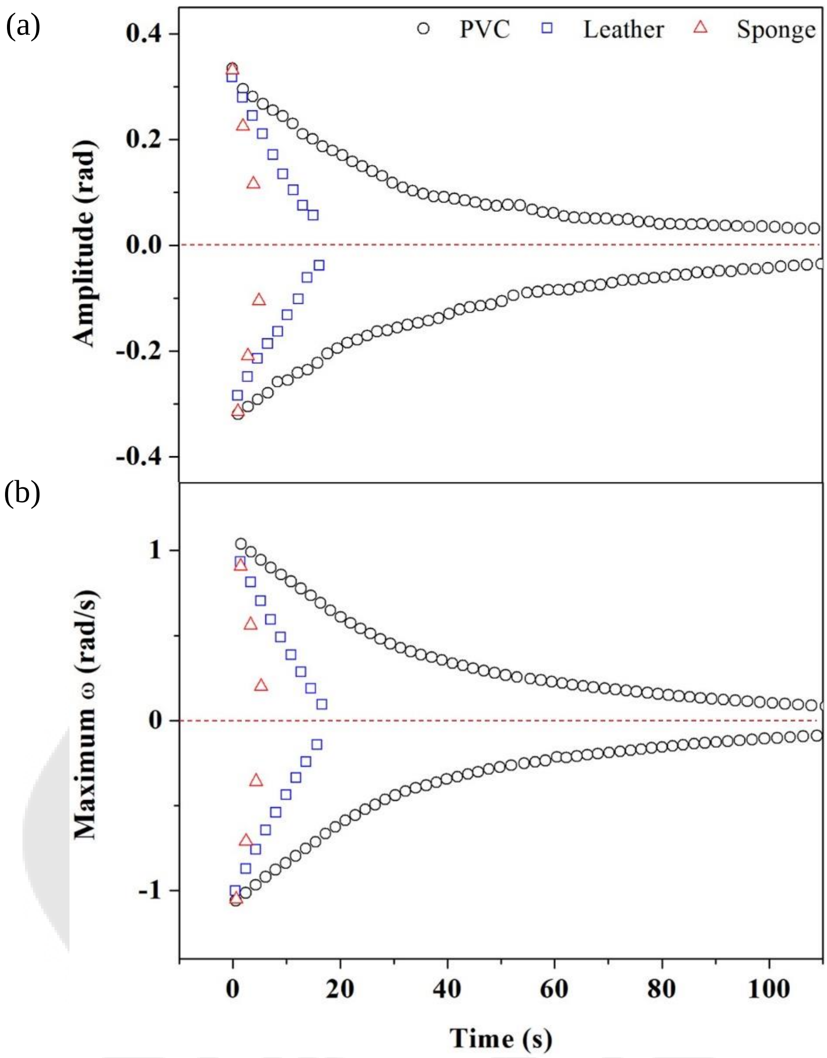

Figure 17. (a) Amplitude and (b) maximum ω as a function of time for the cylindrical pipe with and without synthetic leather or sponge.

Figure 18 represents the coefficient of rolling friction μ_r as a function of the cylindrical pipe's velocity at the middle of the track in each cycle. These μ_r were calculated from the relation $\left(D_{d(n)}/R_c\right)\Big/\left(1+I/MR_c^2\right)$ and $\left(D_{u(n)}/R_c\right)\Big/\left(1+I/MR_c^2\right)$ for rolling down and up, respectively. The values of the coefficient of rolling friction calculated for the uncovered cylindrical pipe rolling down and up are similar. However, these values are different, but they follow the same trend for the cylindrical pipe with synthetic leather or sponge. The coefficient of rolling friction values are dependent on the cylindrical pipe's velocity for the cylindrical pipe with synthetic leather or sponge. Normally, these values are proportional to the velocity of the cylindrical pipe. However, it is different for the uncovered cylindrical pipe. The values of μ_r in a range of $0.30\,\mathrm{m/s} < v < 0.46\,\mathrm{m/s}$, is similar and quite small, which is about 0.0027 ± 0.0007. When v decreases in a range of $0.15\,\mathrm{m/s} < v < 0.30\,\mathrm{m/s}$, the coefficient of rolling friction slightly increases and reaches a maximum value of 0.0095 ± 0.0005 at $v = 0.15$ m/s. Notice that the rolling friction is less affected in the velocity range of $0.30\,\mathrm{m/s} < v < 0.46\,\mathrm{m/s}$, and it plays an important role at the lower velocity range of $0.15\,\mathrm{m/s} < v < 0.30\,\mathrm{m/s}$. When v is lower than $0.15\,\mathrm{m/s}$, the coefficient of rolling friction linearly decreases as the uncovered cylindrical pipe's velocity decreases. It can be seen that the rolling friction is very small if the uncovered cylindrical pipe rolls with enough velocity. For the synthetic leather cylinder, the surface of the synthetic leather is quite rough, and the material is hard. In the beginning of the synthetic leather cylinder rolling at a velocity in a range of $0.28\,\mathrm{m/s} < v < 0.44\,\mathrm{m/s}$, The values of μ_r are similar, which is about 0.0082 ± 0.0006. Meanwhile, the synthetic leather cylinder oscillates with low v, which is $0.28\,\mathrm{m/s}$, in the 4th cycle of rolling, and the rolling friction has managed to further reduce the angular velocity. The coefficient of rolling friction then rapidly drops to about 0.0083 and 0.0043 for the synthetic leather cylinder rolling down. Notice that in a velocity range of $0.15\,\mathrm{m/s} < v < 0.28\,\mathrm{m/s}$, The values of μ_r is linearly dependent on the velocity of the synthetic leather cylinder. The sponge cylinder oscillates just three cycles. Similarly, the values of μ_r are proportional to the sponge cylinder's velocity. Furthermore, it can be seen that the values of μ_r for the uncovered cylindrical pipe rolling down and up are similar. While, these values for the cylindrical pipe rolling down are larger than that for the cylindrical pipe rolling up in case of the cylindrical pipe with synthetic leather or sponge, especially sponge. Since the coefficient of rolling friction is dependent on the values of D_d and D_u, and the cylindrical pipe with a soft surface can be easily deformed. When it is rolling down, there is only a torque exerted by N for reducing the angular velocity, possibly a distance of D_d for rolling down is larger than D_u for rolling up. The experiment is simple and is suitable for determining the coefficient of rolling friction. Moreover, it will help students to better understand the rolling friction effect of the rolling object.

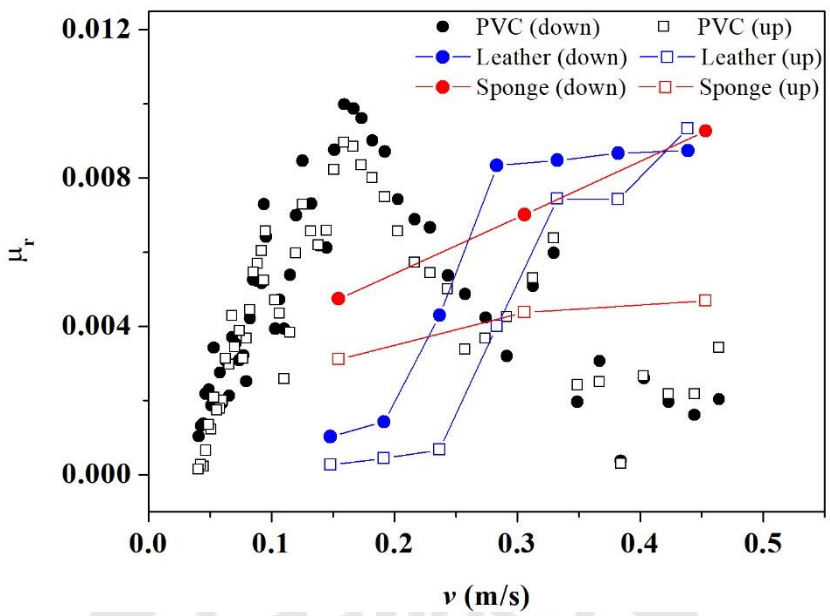

Figure 18. Parameter μ_r as a function of the cylindrical pipe's velocity v at the middle of the track for the cylindrical pipe with and without synthetic leather or sponge.

CHAPTER 5
SUMMARY DISCUSSION AND SUGGESTION

5.1 Summary

We have demonstrated the use of a smartphone sensor for estimating the coefficient of rolling friction of a cylindrical pipe with and without synthetic leather or sponge rolling on a curved aluminum track. Rolling Cylinder application simultaneously recorded the angular position and angular velocity of the cylindrical pipe, and all experimental data were analyzed for estimating the coefficient of rolling friction. The results show that the values of the coefficient of rolling friction are dependent on the velocity of the cylindrical pipe with synthetic leather or sponge surface. However, the coefficient of rolling friction is less affected at high velocity ($0.30\,\mathrm{m/s} < v < 0.46\,\mathrm{m/s}$) for the uncovered cylindrical pipe. It is inversely proportional to the cylindrical pipe's velocity (in a range of $0.15\,\mathrm{m/s} < v < 0.30\,\mathrm{m/s}$) and become linearly dependent on the uncovered cylindrical pipe's velocity at low speed ($v < 0.15\ \mathrm{m/s}$). This experiment is simple and easy to perform for recording experimental data in a physics laboratory. The experiment is suitable for teaching mechanics at the level of undergraduate students. It will help students better understand the effect of rolling friction on rolling objects.

5.2 Discussion

For our experiment, the cylindrical pipe's surfaces are not smooth. In the case of rolling on the track, the resultant reaction force N is assumed that it acts to the cylindrical pipe ahead of its center of mass, shifted by a small distance D_d or D_u for rolling down and up, respectively. A torque ND_d or ND_u is in opposite direction to the angular velocity of the cylindrical pipe in order to resist the rolling motion. These D_d and D_u values are used to calculate the coefficient of rolling friction from $\mu = f/N$. According to the calculation, there are 2 terms for μ. The 1st term depends on the angle of inclination for the cylindrical pipe rolling on an inclined plane. Nevertheless, we focus on the 2nd term, which is associated with D_d and D_u values. These are $\mu_r = \left(D_d/R_c\right)\Big/\left(1+I/MR_c^2\right)$ and $\mu_r = \left(D_u/R_c\right)\Big/\left(1+I/MR_c^2\right)$ for rolling down and up, respectively.

In the experiment, the cylindrical pipe with synthetic leather and sponge were released at a same position on the curved track. The experimental results for the cylindrical pipe with and without synthetic leather or sponge are shown. It is clear that the cylindrical pipe with sponge has decreased θ and ω in the 3rd cycle. This is because the sponge surface is softer and thicker, that it can be easily deformed. While, θ and ω of the cylindrical pipe with synthetic leather gently decrease with time because of its roughness. The effect of its thickness can be ignored, since the synthetic leather surface is very thin. In contrast, θ and ω of the uncovered cylindrical pipe slightly decline, since the surface is quite smoother. However, all cylindrical pipes will eventually stop rolling as a result of the frictional force at the contact area. Furthermore, we show the plot of the amplitude and the maximum ω with respect to time for the cylindrical pipe with various surfaces. The amplitude and maximum ω linearly decrease within $20\,\mathrm{s}$ and $7\,\mathrm{s}$ for the cylindrical pipe with synthetic leather and sponge, respectively. While they exponentially decrease within $120\,\mathrm{s}$ for the uncovered cylindrical pipe. Implying, the deformation plays a more important role to resist the rolling motion especially the soft surface, like the sponge surface.

Finally, the coefficient of rolling friction was calculated in each rolling cycle, and then the coefficient of rolling friction as a function of the cylindrical pipe's velocity was estimated. The values of the coefficient of rolling friction are directly dependent on the velocity for the cylindrical pipe with synthetic leather or sponge. However, the values of coefficient of rolling friction are quite stable at high velocity ($0.30\,\mathrm{m/s} < v < 0.46\,\mathrm{m/s}$) for the uncovered cylindrical pipe, and then it increases as the cylindrical pipe's velocity decreases (in a range of $0.15\,\mathrm{m/s} < v < 0.30\,\mathrm{m/s}$). Eventually, the values of the coefficient of rolling friction of the uncovered cylindrical pipe become linearly proportional to the velocity ($v < 0.15\ \mathrm{m/s}$). Therefore, the cylindrical pipe's surface is a significant factor for estimating the coefficient of rolling friction.

5.3 Suggestion

This research demonstrated the use of a smartphone sensor for estimating the coefficient of rolling friction of the cylindrical pipe with various surfaces rolling on the curved aluminum track. We applied a smartphone to be a part of our experimental setup to collect the experimental data. Therefore, this experiment is low-cost and suitable for students. In order to improve this experiment, the additional experiment should be done as follows,

1. A high quality device such as a high speed camera may be used to detect the motion of the cylindrical pipe for improving the accuracy in the calculated coefficient of rolling friction.

2. Various surfaces of the cylindrical pipe and the track may be applied to this experiment for studying the relation between the surfaces and the rolling motion.

3. Other factors, beside the effect of the surface may be considered for estimating the coefficient of rolling friction, such as the size of the cylindrical pipe or the track, the material of the cylinder.

REFERENCES

Ambrosis, A. D., Malgieri, M., Mascheretti, P., & Onorato, P. (2015). Investigating the role of sliding friction in rolling motion: a teaching sequence based on experiments and simulations. *European Journal of Physics, 36*(3), 035020.

Arabasi, S., & Al-Taani, H. (2016). Measuring the Earth's magnetic field dip angle using a smartphone-aided setup: a simple experiment for introductory physics laboratories. *European Journal of Physics, 38*(2), 025201.

Cross, R. (2015a). Effects of surface roughness on rolling friction. *European Journal of Physics, 36*(6), 065029.

Cross, R. (2015b). Rolling to a stop down an inclined plane. *European Journal of Physics, 36*(6), 065047.

Cross, R. (2015c). Why low bounce balls exhibit high rolling resistance. *Physics Education, 50*(6), 717-721.

Cross, R. (2016). Coulomb's law for rolling friction. *American Journal of Physics, 84*(3), 221-230.

Cross, R. (2017). Rolling Uphill. *The Physics Teacher, 55*(4), 221-221.

Cross, R. (2018). Effects of rolling friction on a spinning coin or disk. *European Journal of Physics, 39*(3), 035005.

de Jesus, V. L. B., Pérez, C. A. C., de Oliveira, A. L., & Sasaki, D. G. G. (2018). Understanding the gyroscope sensor: a quick guide to teaching rotation movements using a smartphone. *Physics Education, 54*(1), 015003.

Egri, S., & Szabó, L. (2015). Analyzing Oscillations of a Rolling Cart Using Smartphones and Tablets. *The Physics Teacher, 53*(3), 162-164.

Kapucu, S. (2018). A simple experiment to measure the maximum coefficient of static friction with a smartphone. *Physics Education, 53*(5), 053006.

Minkin, L., & Sikes, D. (2018). Coefficient of rolling friction - Lab experiment. *American Journal of Physics, 86*(1), 77-78.

Mungan, C. E. (2012). Rolling friction on a wheeled laboratory cart. *Physics Education, 47*(3), 288-292.

Phommarach, S., Wattanakasiwich, P., & Johnston, I. (2012). Video analysis of rolling cylinders. *Physics Education, 47*(2), 189-196.

Pörn, R., & Braskén, M. (2016). Interactive modeling activities in the classroom—rotational motion and smartphone gyroscopes. *Physics Education, 51*(6), 065021.

Puttharugsa, C., Khemmani, S., Utayarat, P., & Luangtip, W. (2016). Investigation of the rolling motion of a hollow cylinder using a smartphone. *European Journal of Physics, 37*(5), 055004.

Serway, R. A., & Jewett, J. W. (2004). *Physics for Scientists and Engineers* (6).

Stolarski, T. A. (1990). 6 - Friction, lubrication and wear in higher kinematic pairs T. A. Stolarski *Tribology in Machine Design* (pp. 232-247): Newnes.

Vogt, P., & Kuhn, J. (2012). Analyzing free fall with a smartphone acceleration sensor. *Phys. Teach., 50*(3), 182-183.

Vozdecký, L., Bartoš, J., & Musilová, J. (2014). Rolling friction—models and experiment. An undergraduate student project. *European Journal of Physics, 35*(5), 055004.

Wattanayotin, P., Puttharugsa, C., & Khemmani, S. (2017). Investigation of the rolling motion of a hollow cylinder using a smartphone's digital compass. *Physics Education, 52*(4), 045009.

Yan, Z., Xia, H., Lan, Y., & Xiao, J. (2017). Variation of the friction coefficient for a cylinder rolling down an inclined board. *Physics Education, 53*(1), 015011.

Appendix

A. Rolling without slipping for the uncovered cylindrical pipe

We released the uncovered cylindrical pipe at the position $s_0 = 0.15 \pm 0.02\,\mathrm{m}$ as shown in Fig.14. To confirm the rolling without slipping situation, we recorded a video to observe the uncovered cylindrical pipe rolling on the curved track. The video is in a link below: https://drive.google.com/open?id=1_3PzAp-_hfu9EvhXJRPqoSGTi0m9QxGV. Also, we used Tracker program to track the uncovered cylindrical pipe's movement in the video (Figure A1). The calculated distance s_0 in the first rolling down was about $0.149\ \mathrm{m}$ which was close to the setting distance. Therefore, there is no slipping for this situation.

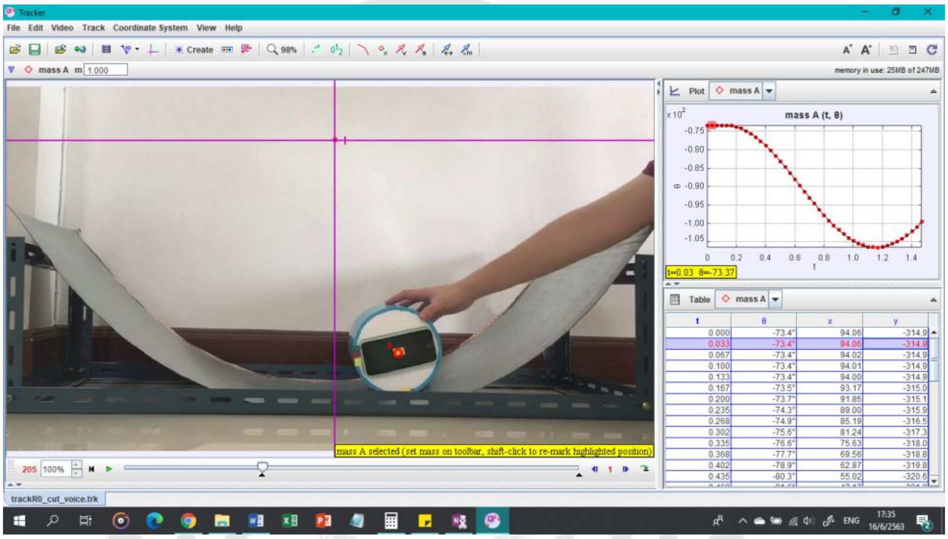

Figure A1. Tracker program for measuring the distance s_0 of the uncovered cylindrical pipe (from the right side to the middle of the curved track in the first rolling down)

B. Experimental data

The experimental results with 3 repeats in each surfaces are shown in this section. It includes

1. Angular displacement θ and angular velocity ω with time (1^{st} – 3^{rd} experiment).

2. The relation between the coefficient of rolling friction μ_r and the velocity v of the cylindrical pipe at the middle of the track.

1. The cylindrical pipe with a synthetic leather.

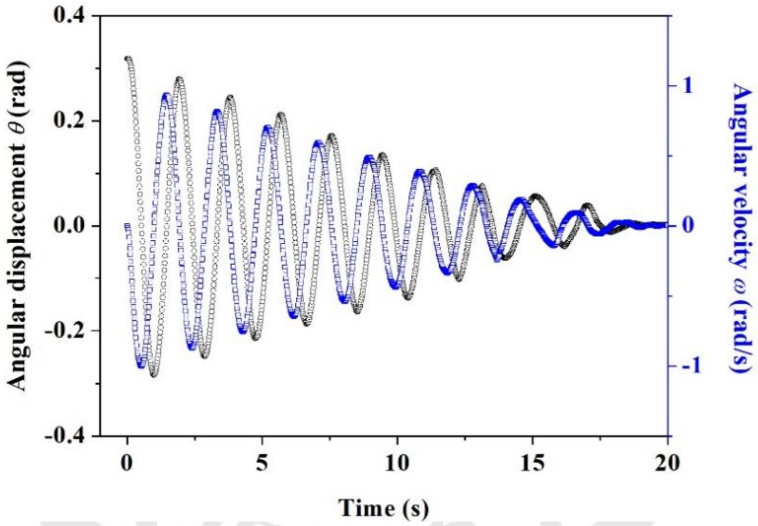

Figure B1. Angular displacement θ and angular velocity ω with time for a cylindrical pipe with synthetic leather (1^{st} experiment).

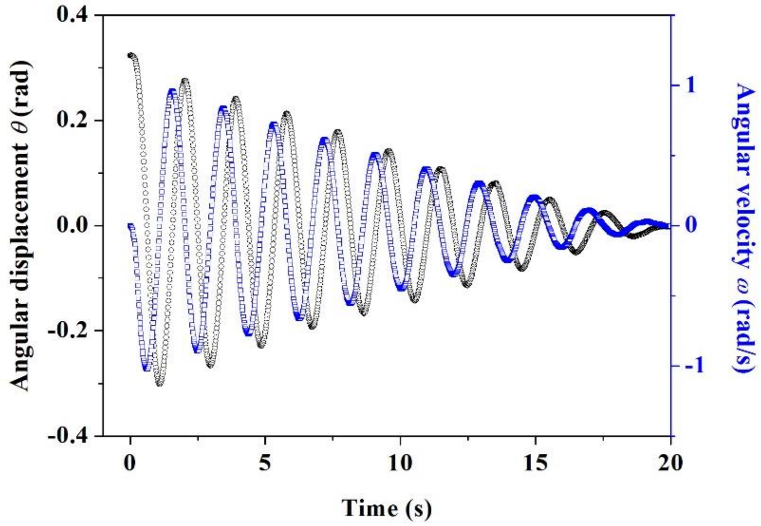

Figure B2. Angular displacement θ and angular velocity ω with time for a cylindrical pipe with synthetic leather (2nd experiment).

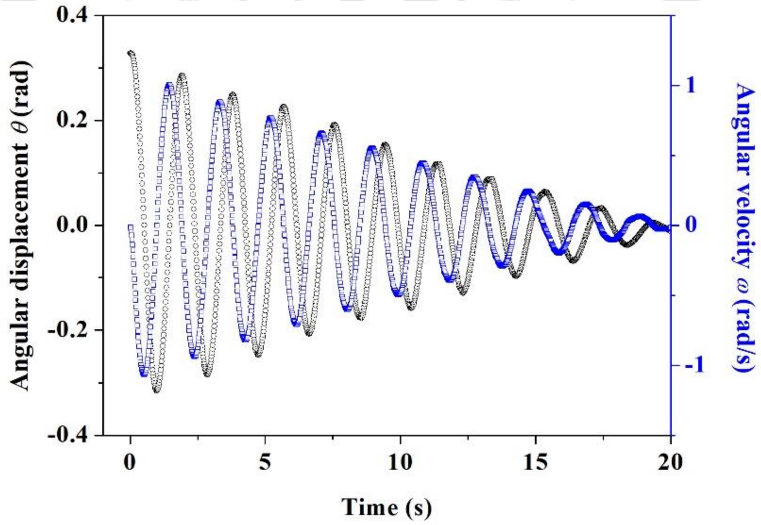

Figure B3. Angular displacement θ and angular velocity ω with time for a cylindrical pipe with synthetic leather (3rd experiment).

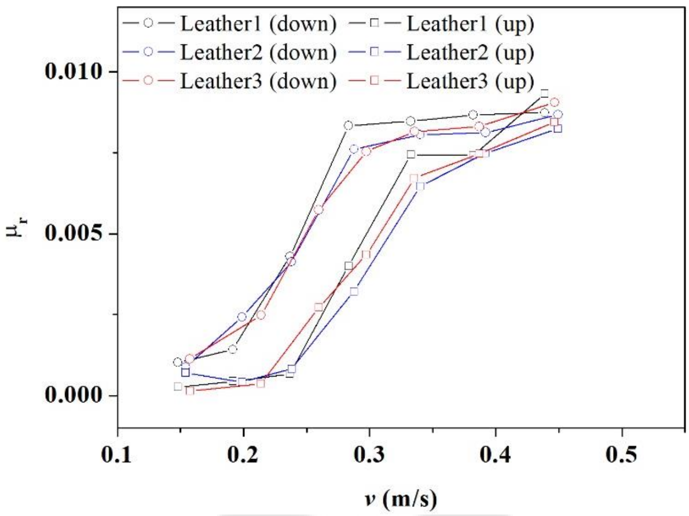

Figure B4. The comparison of the coefficient of rolling friction μ_r vs. velocity v of a synthetic leather cylinder at the middle of the track (3 times).

2. The cylindrical pipe with a sponge.

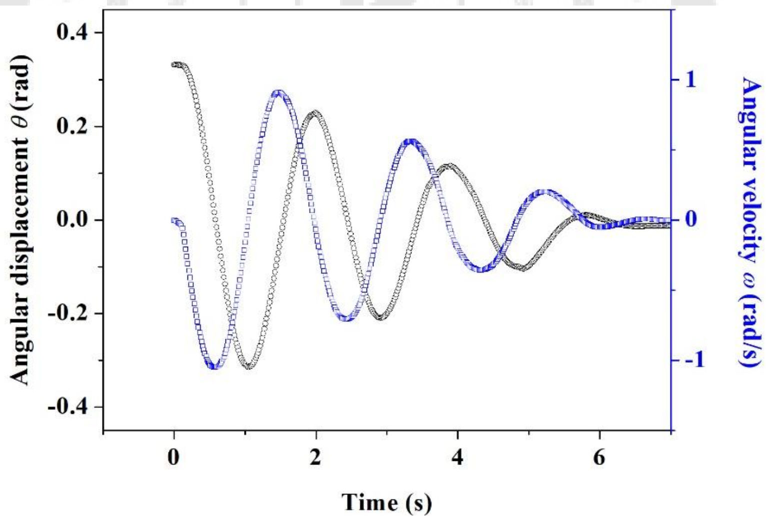

Figure B5. Angular displacement θ and angular velocity ω with time for a cylindrical pipe with sponge (1st experiment).

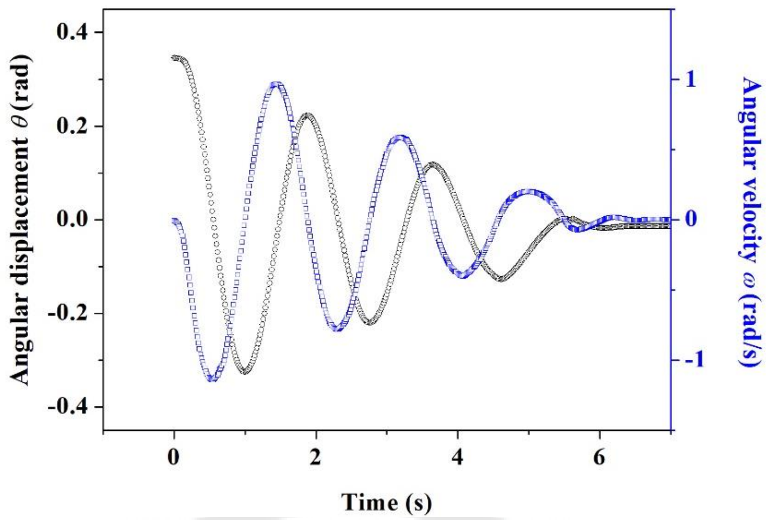

Figure B6. Angular displacement θ and angular velocity ω with time for a cylindrical pipe with sponge (2^{nd} experiment).

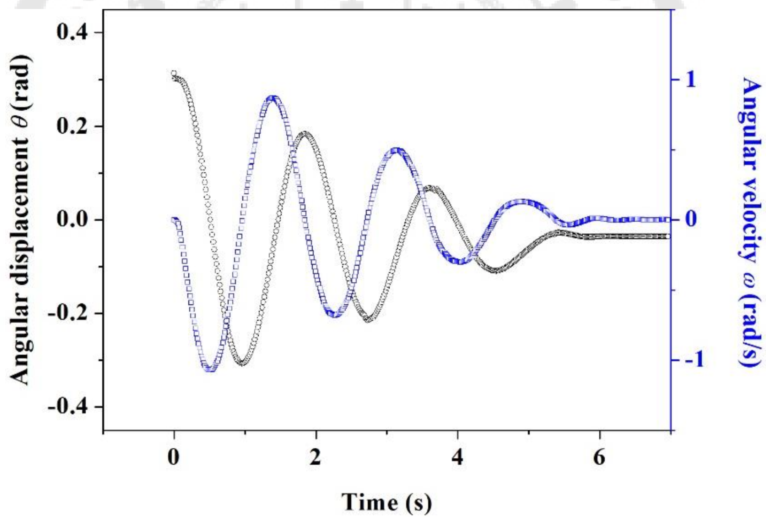

Figure B7. Angular displacement θ and angular velocity ω with time for a cylindrical pipe with sponge (3^{rd} experiment).

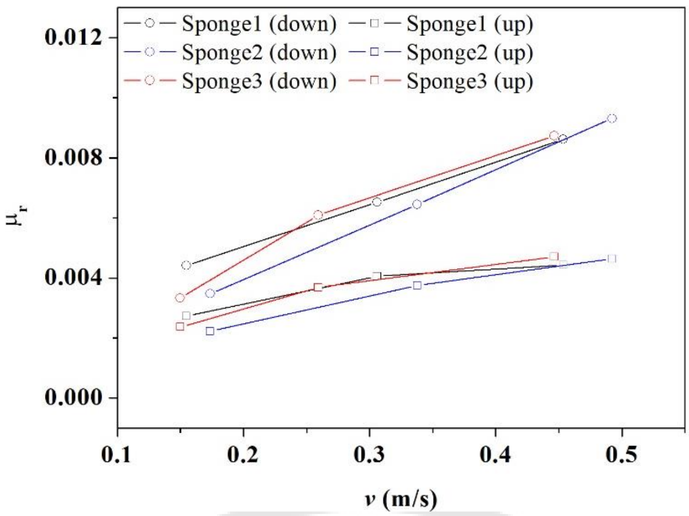

Figure B8. The comparison of the coefficient of rolling friction μ_r vs. velocity v of a sponge cylinder at the middle of the track (3 times).

3. The uncovered cylindrical pipe.

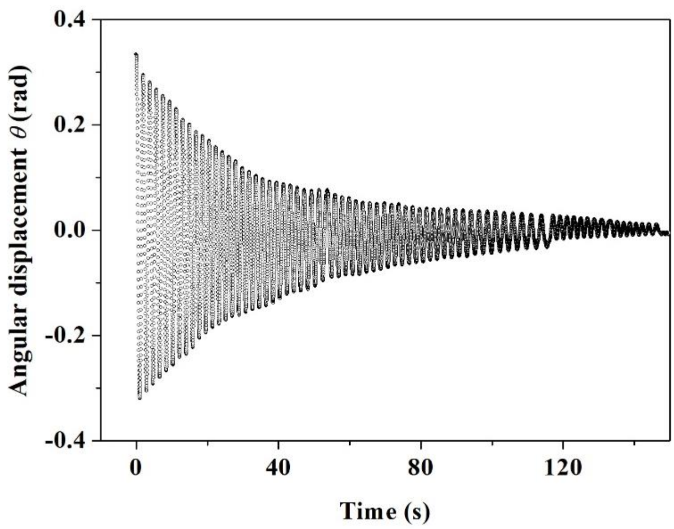

Figure B9. Angular displacement θ with time of an uncovered cylindrical pipe (1st experiment).

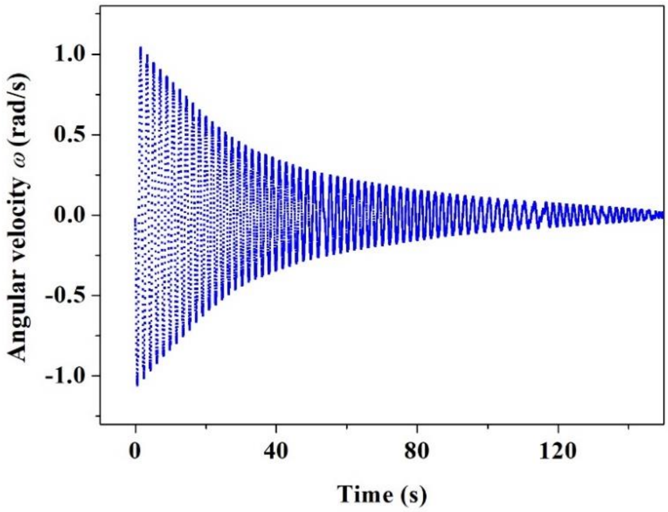

Figure B10. Angular velocity ω with time of an uncovered cylindrical pipe (1st experiment).

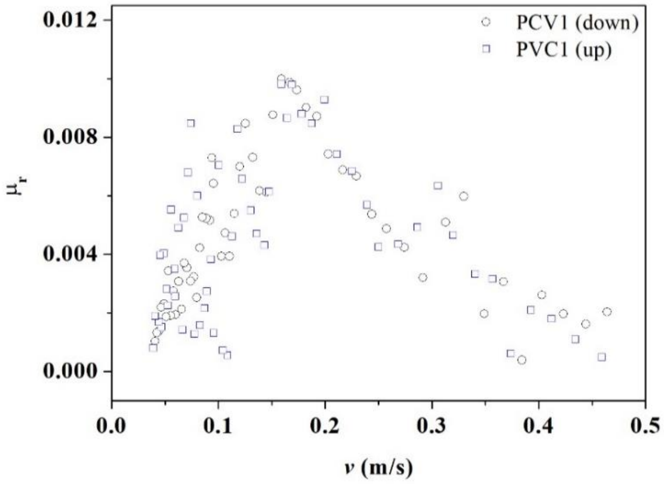

Figure B11. The coefficient of rolling friction μ_r vs. velocity v of an uncovered cylindrical pipe at the middle of the track (1st experiment).

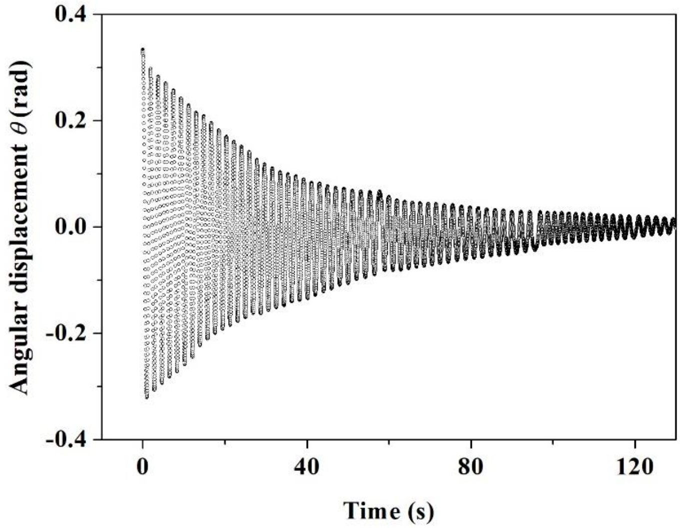

Figure B12. Angular displacement θ with time of an uncovered cylindrical pipe (2^{nd} experiment).

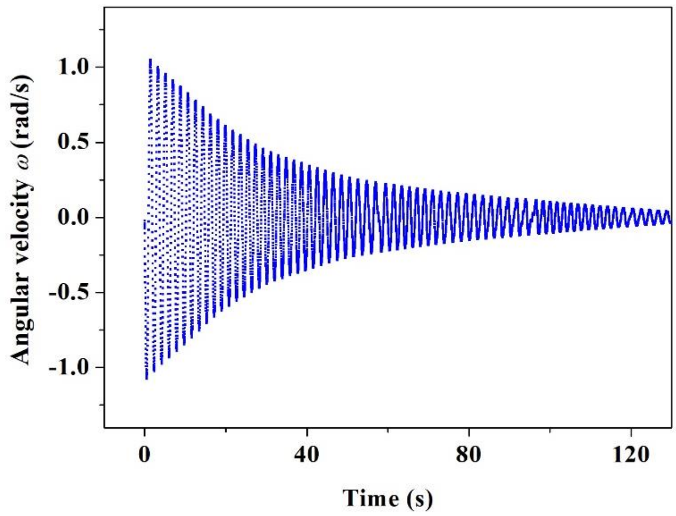

Figure B13. Angular velocity ω with time of an uncovered cylindrical pipe (2^{nd} experiment).

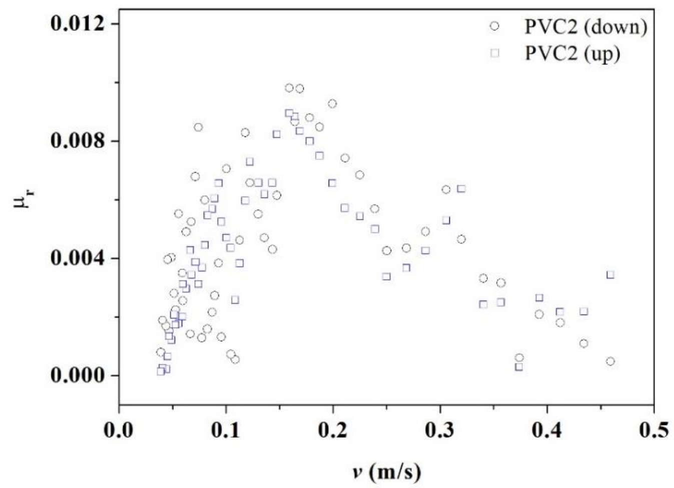

Figure B14. The coefficient of rolling friction μ_r vs. velocity v of an uncovered cylindrical pipe at the middle of the track (2nd experiment).

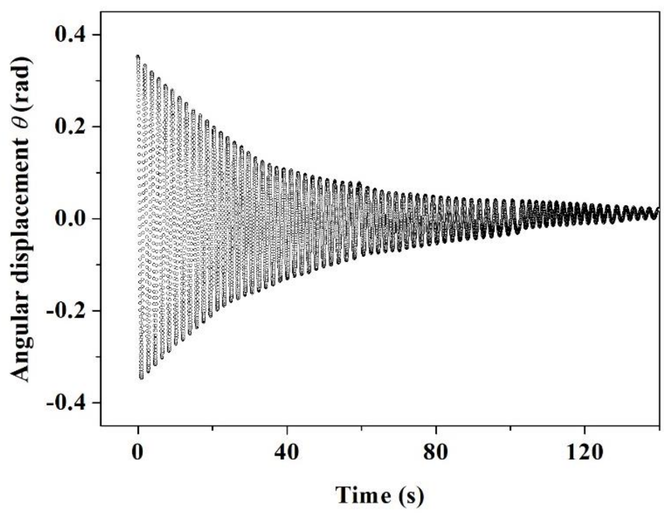

Figure B15. Angular displacement θ with time of an uncovered cylindrical pipe (3rd experiment).

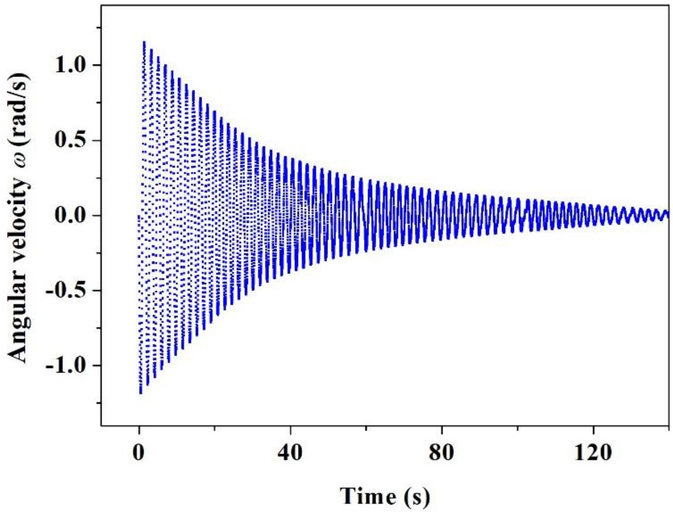

Figure B16. Angular velocity ω with time of an uncovered cylindrical pipe (3rd experiment).

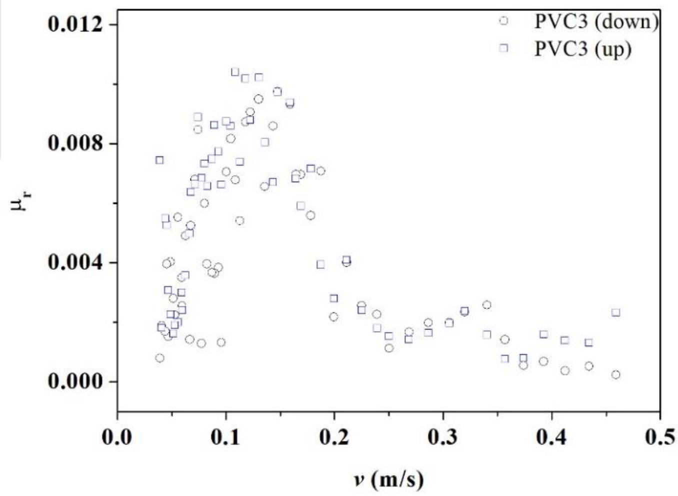

Figure B17. The coefficient of rolling friction μ_r vs. velocity v of an uncovered cylindrical pipe at the middle of the track (3rd experiment).

VITA

NAME	Pimpakarn Laotreephet
DATE OF BIRTH	28 February 1996
PLACE OF BIRTH	Bangkok
INSTITUTIONS ATTENDED	2013 High School : Kanjanapisek Wittayalai Nakhon Pathom School, Nakhon Pathom. 2017 Bachelor Degree : Mahidol University, Nakhon Pathom. 2019 Master Degree : Srinakharinwirot University, Bangkok.
HOME ADDRESS	112/165 Kanjanapisek Rd, Lak Song, Bangkae, Bangkok, 10160.